NOTICE

The quality of this microform is heavily dependent upon the quality of the original thesis submitted for microfilming. Every effort has been made to ensure the highest quality of reproduction possible.

If pages are missing, contact the university which granted the degree.

Some pages may have indistinct print especially if the original pages were typed with a poor typewriter ribbon or if the university sent us an inferior photocopy.

Reproduction in full or in part of this microform is governed by the Canadian Copyright Act, R.S.C. 1970, c. C-30, and subsequent amendments.

AVIS

La qualité de cette microforme dépend grandement de la qualité de la thèse soumise au microfilmage. Nous avons tout fait pour assurer une qualité supérieure de reproduction.

S'il manque des pages, veuillez communiquer avec l'université qui a conféré le grade.

La qualité d'impression de certaines pages peut laisser à désirer, surtout si les pages originales ont été dactylographiées à l'aide d'un ruban usé ou si l'université nous a fait parvenir une photocopie de qualité inférieure.

La reproduction, même partielle, de cette microforme est soumise à la Loi canadienne sur le droit d'auteur, SRC 1970, c. C-30, et ses amendements subséquents.

A Wideband Magnetic Field Probe with Particular Emphasis on Low Frequency Characteristics

by

Mondher Frikha

A thesis submitted to the
School of Graduate Studies and Research
in partial fulfilment of the requirements
for the degree

Master of Applied Science

Ottawa-Carleton Institute for Electrical Engineering
Department of Electrical Engineering
Faculty of Engineering
University of Ottawa
April 1991

ISBN 0-315-68091-1

UNIVERSITÉ D'OTTAWA
UNIVERSITY OF OTTAWA

I hereby declare that I am the sole author of this thesis.

I authorize The University of Ottawa to lend this thesis to other institutions or individuals for the purpose of scholarly research.

Mondher Frikha

I further authorize The University of Ottawa to reproduce this thesis by photocopying or by other means, in total or in part, at the request of other institutions or individuals for the purpose of scholarly research

Mondher Frikha

To my family

ABSTRACT

Measurement of transients of ambient power-line frequency magnetic fields is becoming increasingly important because of the possibility that exposure to such fields may produce effects to communication systems and various electronic devices as well as human health.

Many studies have been concerned with magnetic field measurements over a wide frequency range but small attention has been paid to the measurement of transient fields.

The objective of this study is to investigate the feasibility of developing a magnetic field probe operating in a broad frequency range, including the power line frequency (60 Hz), which would also be suitable for measurements of transient fields (their magnitude and phase). The sensor was modeled, simulated using computer simulation and finally designed. Its performance was tested in time and frequency domains. The sensor, which provides constant amplitude and phase response from 30 Hz to around 5 MHz for the magnetic field, has a minimal response to the electric field (30 dB or less), a sensitivity of 0.48 V/A m^{-1} and wide dynamic range (greater than 40 dB).

ACKNOWLEDGEMENT

I wish to express my gratitude to Dr. D. T. Gibbons for his continuous encouragement and invaluable suggestions throughout the research. I'm also grateful to Dr. M. Stuchly who offered helpful suggestions for much of this work.

The encouragement and motivational help of many, most importantly Dr. S. Stuchly, Dr. A. Thansandote and Mr. H. LePocher is gratefully acknowledged.

A special thanks to Drs. C. H. Chan and G. Costache for reading this thesis and their suggestions and encouragements.

Finally, I would like to express my sincere gratitude to my family to whom this thesis is dedicated. Special thanks goes to the Tunisian government for its scholarship program.

Contents

List of Tables

List of Figures

Notation

Various symbols, superscripts, subscripts, accents and abbreviations used frequently in this work are summarized below. All notation is fully defined where it first arises in the text.

Symbols

a	radius of the wire of the loop.
A_{cm}	common mode gain of the operational amplifier.
A_d	differential gain of the operational amplifier.
A_e	effective cross sectional area of the loop.
A_L	normalized inductance per turn.
A_0	dc open loop gain of the operational amplifier.
A_w	cross sectional area of the winding.
b	diameter of solenoid coil.
b_w	winding width.
C_a	loop interwinding capacitance.
C_1	toroidal core factor.
d_2	outer diameter of the toroid of the transformer.
d_1	inner diameter of the toroid of the transformer.
E_{TEM}	electric field amplitude inside the TEM cell.
E_i	electric field incident to the loop antenna.
f_{sens}	low cut-off frequency of the loop antenna.
f_{ti}	low cut-off frequency of transformer of stage i.
H	magnetic field intensity.
h	height of the toroid.
H_{TEM}	magnetic field intensity inside the TEM cell.

h_e effective height.

h_w winding height.

i_b input bias current of the operational amplifier.

K Nagoaka's constant.

L_a inductance of the loop antenna.

l_c length of the solenoid coil.

l_e effective length of the magnetic circuit.

l_{en} total length of the conductor of the loop.

L_{li} equivalent leakage inductance of the

L_{pi} open circuit parallel inductance of the transformer of stage i.

L_{sei} open circuit series inductance of the transformer of stage i.

l_w length of one toroidal turn. of stage i.

N_a number of loop turns.

N_{ti} turn ratio of transformer of stage i.

P_{TEM} power entering the TEM cell.

R_a winding resistance of the loop antenna.

R_f feedback resistor of the current follower.

R_{ic} resistance per unit length of the wire of gauge i.

R_{in} open loop input impedance of the operational amplifier.

R_L loading resistance.

R_{pi} magnetic loss resistor of the transformer of stage i.

R_{sei} open circuit series resistance of the transformer of side i.

R_{wa} resistance per unit length of the conductor of the loop.

R_{wi} total winding resistance of the transformer of stage i.

R_{wt} resistance per unit length of the wire of the transformer.

V_c output voltage of the transimpedance amplifier.

T_0	resistor tolerance.
V_{oc}	induced open circuit voltage.
V_{os}	input offset voltage of the operational amplifier.
Z_{amp}	Input impedance of the current follower.

Greek Letters

β	propagation constant, $\beta = 2\pi/\lambda$.
λ	wavelength.
μ_0	permeaility of the free space.
μ_i	initial permeaility of the core material.
μ_c	effective permeability of the coil.
μ_e	effective permeability of the magnetic circuit.
ω_0	pole angular frequency of the operational amplifier.
ρ	resistivity of the copper wire.
τ	time constant.

Acronyms and Definitions

AWG	American wire gauge.
BW	bandwidth.
CML	cylindrical Moebius loop.
CMRR	common mode rejection ratio.
DUT	device under test.
EM	electromagnetic.
EMI	electromagnetic interference.
EMP	electromagnetic pulse.
ESD	electrostatic discharge.
MGL	multi-gap loop.
MTL	multi-turn loop.
NA	network analyzer.
rms	root mean square.
TEM	transverse electromagnetic.

Chapter 1

Introduction

Natural and man made electromagnetic (EM) transients such as lightning, electrostatic discharge (ESD), nuclear electromagnetic pulse (EMP) and those associated with high power switching have broad frequency spectra. They can cause electromagnetic interference (EMI) with communication systems and various electronic devices. Over the years, research has been conducted to characterize the electromagnetic fields due to these transient sources [3-9], [42]. Most studies have been aimed at finding protection techniques and establishing design guidelines to minimize susceptibility of telecommunication and electronic equipment. Characterization of such transient fields requires electric and magnetic field sensors to measure both the magnitude and phase of the field. The sensing device of such sensors is usually an electrically small antenna. These antennas are considered small since their size is a small fraction of the signal wavelength. This feature provides both a higher degree of spatial resolution and small perturbation of the electric field.

1.1 Motivation

Many EM field sensors have been developed over the years. In many cases attention has been focused on the high frequency performance (above 500 MHz) [42]. Most sensors respond to the electric field. Recently, a broadband high frequency magnetic field sensor has been developed by a group of researchers at the University of Ottawa [27].

Biomedical research has raised the possibility that exposure to low level electric and magnetic fields of low frequencies may affect cancer development and cause other biological effects [39]. Some of the data indicate that the field waveform, and specifically transient or pulsed fields, may be of importance [28]. Various pulsed low frequency magnetic fields are also used in medicine for diagnostic and therapeutic applications [50]. Hence, there is a need to characterize such fields.

This need for a magnetic field sensor suitable for measurements of transients and pulsed fields at frequencies extending below the power line frequency (60 Hz), and the limitations of existing sensors have provided the motivation for this work. Furthermore, it was felt that modern integrated circuits and simulation techniques would offer suitable tools for optimization of the design.

1.2 Objective

The objective of this thesis is to analyse and optimize the performance of a magnetic field sensor similar to that described by Stuchly, *et al.* [27], but suitable

for operation below 60 Hz. The design of a magnetic field sensor should meet the following requirements:

- Wide-band performance with a low cutoff frequency (below 60 Hz).
- Frequency independent transfer function within the range of operation.
- Minimum perturbation of the measured fields.
- Well defined directional response.
- Wide dynamic range.
- High sensitivity
- Minimal response to the electric field.

The selected design is to be evaluated in the frequency and time domains.

1.3 Thesis Organization

In Chapter 2, the basic concepts of the small loop antenna are outlined and a critical literature review of different kinds of magnetic field sensor that have been previously described is provided.

In Chapter 3, the low frequency limitations of a magnetic field sensor that was built recently at the University of Ottawa [27] are given. The sensor performance at low frequencies is described and modelled. The sensor's cutoff frequencies are

derived. A simulation was carried out to show that, for specific design parameters, the low cut-off frequency of the magnetic field sensor is determined by that of the loop antenna. An attempt was made afterward to optimize the design of the loop antenna in order to reduce further its low cut-off frequency. A non-linear optimization technique was used to show the low frequency limitations of such a design. It was shown that the magnetic field sensor had to be redesigned to achieve the desired low frequency performance.

In Chapter 4, the structure of the loop is modified to obtain a magnetic field sensor suitable for measuring fields below 60 Hz. This design is based on a multi-turn antenna (solenoid) with a ferrite core, a balanced transformer, and an instrumentation amplifier. Design criteria for each part of the magnetic field sensor are given to justify the choice of the different components that have been used.

In Chapter 5, the performance of the magnetic field sensor is investigated. The magnetic field sensor is modeled, then its performance is analyzed in both time and frequency domains by using Hspice simulation. Measurements of the sensor output parameters were performed in order to verify the simulated results, and to get a full characterization of the magnetic field sensor.

In Chapter 6, the results are summarized and suggestions for future research are made.

Appendix A gives the procedure for the calculation of the inductance of a multi-turn loop antenna.

In Appendix B, a brief description of a wideband transformer is given.

Appendix C provides more details of the nonlinear optimization method used in Chapter 3 in order to minimize the loop antenna low cut-off frequency.

In Appendix D, the method used to identify the equivalent circuit parameters of the antenna and transformer is presented.

Appendix E contains the listings of all the components values used in the design, data sheets of the operational amplifiers used and the listings of the simulation programs.

Chapter 2

Background and Literature Review

Magnetic field sensors discussed here are electrically small. They are formed by loops with or without a ferromagnetic (ferrite) core. These sensors fall into two groups, active and passive. Over a broad range of frequencies, these sensors should have the following properties:

- **Passive sensors:**

  (i) The sensitivity should be defined in terms of the geometry only, and

  (ii) The impedance should be defined in terms of the geometry only.

- **Active sensors:**

  The transfer function should be defined and simple across a wide frequency band.

Two types of sensor transfer function are possible with, (i) the output proportional to the measured field or, (ii) the output proportional to the time derivative

of the field. Most commercially available sensors of the magnetic field are of the second type, and their response has to be integrated to obtain the actual measured field.

In this Chapter, basic concepts regarding the small loop antenna are outlined, and a critical literature review of different kinds of magnetic field sensors is provided.

2.1 Loop Antenna - Basic Concepts

An accurate characterization of the field in the near field of a radiation source requires the use of small sensors to provide both a high degree of spatial resolution and small perturbation to the field from the presence of the sensor [47]. An ideal magnetic field sensor for this purpose would be an infinitesimal magnetic dipole, of which a small loop is considered to be a good approximation. Such a sensor may consist of a single turn loop [20] or a multi-turn loop, e.g. a single-layer solenoid coil [1], [45]. The loop is considered electrically small provided that [17]:

$$l_{en} \leq 0.1\ \lambda \tag{2.1}$$

and,

$$\frac{l_c}{2\,b} \geq 3 \tag{2.2}$$

where:

l_{en} is the total length of the conductor
$l_c/2b$ is the ratio of the length to diameter for a solenoidal coil.

An open circuit voltage developed at the terminals of a small loop placed in an electromagnetic field can be deduced from the Faraday-Maxwell relation [47]:

$$\oint E\, dl = -\frac{\partial}{\partial t} \int_A \mu\, H\, dA \tag{2.3}$$

For harmonic fields, the integral $\oint E\, dl$ evaluated along the loop length results in an open circuit voltage at the terminal:

$$V_{oc} = -j\omega \int_A \mu H\, dA \tag{2.4}$$

Assuming that H is perpendicular to the loop plane and uniform over the loop area, equation (2.4) becomes:

$$V_{oc} = -j\omega\mu H A \tag{2.5}$$

A response of the electric field can also be calculated by expressing V_{oc} in terms of the magnitude of the incident electric field E_i and effective height h_e [17]. For a uniform plane wave with the wave vector $\mathbf{k}$ and orientation as shown in Figure 2.1, using the spherical coordinates, the open circuit voltage can be expressed as [17]:

$$V_{oc} = j\omega N_a A B_i \cos\psi \sin\theta = h_e(\psi, \theta) E_i \tag{2.6}$$

where

$$h_e(\psi, \theta) = j\beta\, N_a \cos\psi sin\theta \tag{2.7}$$

β is the propagation constant of the plane wave, $\beta = 2\pi/\lambda$.

Therefore, the open circuit voltage represents the response to the normal component of the magnetic field, and to the average electric field in the plane of

the loop. In practice, for electrically small loops, response to the E-field is usually quite small so that often it can be ignored.

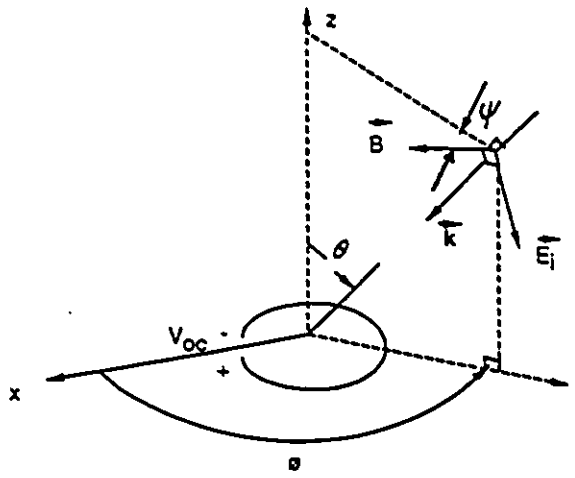

Figure 2.1: Plane-wave field incident on receiving loop

The input impedance of the loop can be expressed as:

$$Z_a = R_a + j\omega L_a \tag{2.8}$$

where

R_a represents the total winding resistance of the loop when the loop radiation resistance is neglected.

L_a is the inductance of the loop antenna.

At low frequencies, the skin depth effect of the winding resistance for single-turn loops and solenoidal coil can be neglected. R_a is then equal to:

$$R_a = R_{wa} \times \textit{total length of conductor} \tag{2.9}$$

where R_{wa} is the resistance per unit length of a straight conductor with the same cross section as the loop conductor.

The self inductance of a small loop of radius b, constructed of wire of radius a can be determined from one of the many formulas available in the literature [26],[51];

- For a single-turn circular loop [26];

$$L_a = \mu_0\, b\, (\ln(\frac{8b}{a}) - 2) \tag{2.10}$$

- For a tightly wound single layer solenoidal coil of length l_c and radius b [51];

$$L_a = \frac{K\, \mu_0\, N_a^2 A}{l_c} \tag{2.11}$$

  where the factor K, known as Nagaoka's constant is shown as a ratio of $l_c/2b$ in Figure 2.2[1]. Appendix A gives more information concerning the loop inductance calculation.

For a magnetic field sensor loaded by a resistance R_L, the Thévenin equivalent circuit is shown in Figure 2.3. The output voltage of the sensor can be written as:

$$V_{out} = \frac{j\omega\mu_0 A_e H R_L}{j\omega L_a + R_L + R_a} \tag{2.12}$$

where A_e is the effective area of the loop antenna.

$A_e = A\ N_a$, where A is the cross-sectional area, and N_a is the number of turns.

[1]This Figure is taken from Antenna Engineering Handbook, Second edition [17],pp. 5-7.

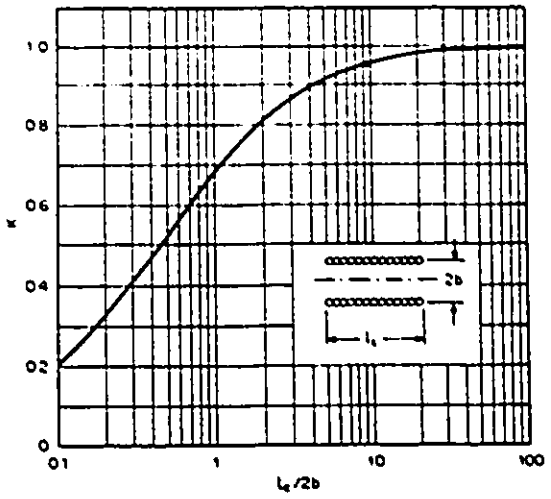

Figure 2.2: Nagaoka's constant vs length to diameter ratio of the loop

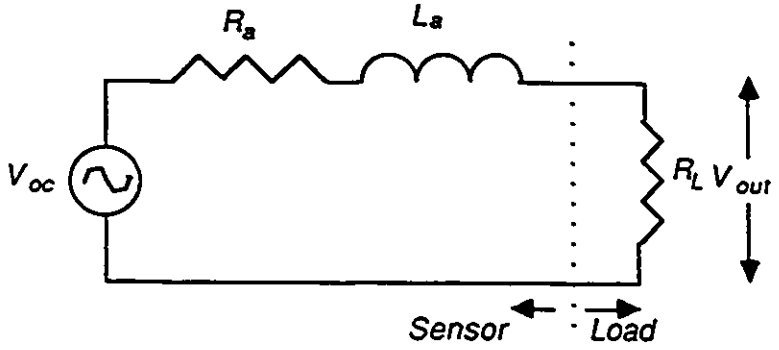

Figure 2.3: Thévenin equivalent circuit of the loop antenna

The magnitude of the output voltage, V_{out} is shown in Figure 2.4 as a function of frequency [22].

Two regions can be identified

- For $R_L + R_a \gg \omega L_a$:

$$V_{out} = j\omega\mu_0 A_e H \tag{2.13}$$

In this case, the output voltage is proportional to the time derivative of the magnetic field.

- For $R_L + R_a \ll \omega L_a$:

$$V_{out} = \frac{\mu_0 A_c H R_L}{L_a} \tag{2.14}$$

In this case, a flat magnitude response is obtained since the output voltage of the sensor is proportional to the magnetic field.

The transition frequency corresponding to the 3dB point is determined by:

$$f_c = \frac{(R_a + R_L)}{2\pi L_a} \tag{2.15}$$

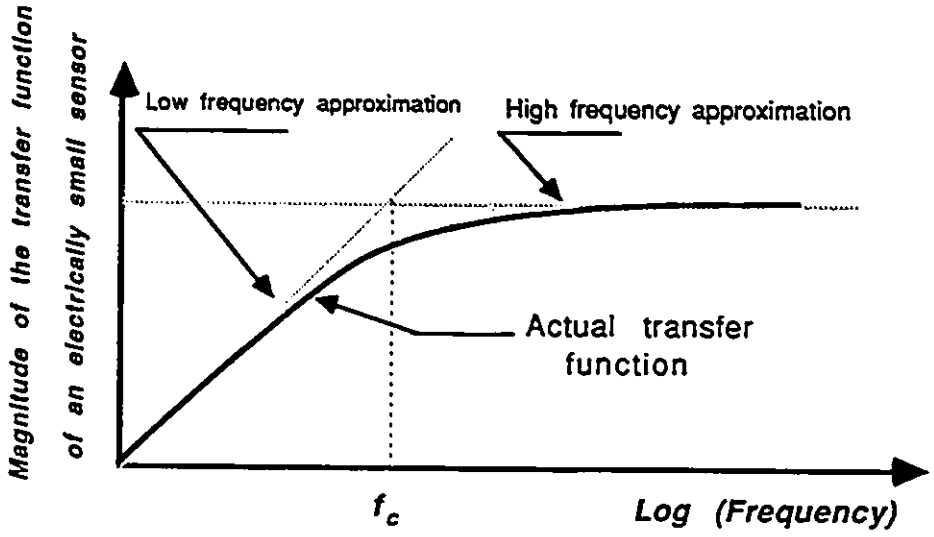

Figure 2.4: Magnitude of the transfer function of an electrically small sensor

If R_L is comparable to R_a, the transition frequency is low and the sensor will produce an output voltage proportional to the magnetic field over a wide

bandwidth.

A sensor output proportional to the magnetic field (flat response) is usually sought. Such kind of sensor does not need external integrators to convert sensor output to a signal proportional to the field (derivative sensors).

2.2 Literature Review

As mentioned earlier, magnetic field sensors can be passive or active. Both types have been described in several publications [3-9], [24], [42]. In this section, a brief overview of the most common sensors is given. Their characteristics and application are outlined.

2.2.1 Passive Magnetic Field Sensors

Passive magnetic field sensors are made with only passive components. They were the first magnetic field sensors to be constructed. They are commonly used in EMP and lightning applications. The major problem found when designing magnetic field sensors is their response to the unwanted electric field. Some work has been carried out in order to overcome this problem. This has led to the development of very elaborated magnetic field sensor geometries [3-9]. Some of the most important ones are discussed below.

Shielded Loop Magnetic Field Sensor

The shielded loop antenna is an example where the electric field is selectively shielded while the magnetic field is unaffected [21]. It is usually made of a coaxial cable the shield of which has been interrupted as shown in Figure 2.5. The gap at the top of the loop helps to discriminate against the predominant electric field. The shielded loop can be shorted at the ground side half-way from the ground plane as shown in Figure 2.6. This configuration, known as shielded half-loop sensor, is commonly used for measurements of magnetic fields tangential to a metal surface.

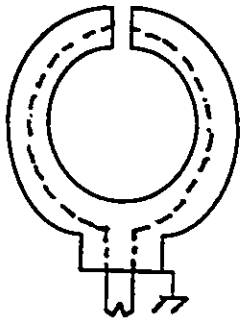

Figure 2.5: Shielded loop antenna

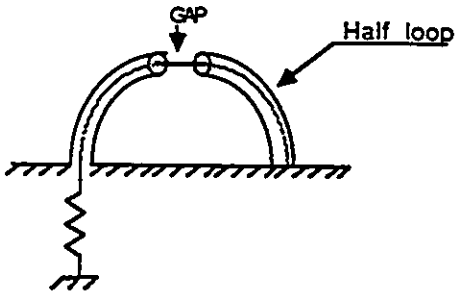

Figure 2.6: Shielded half loop antenna

Moebius Loop

The Moebius loop magnetic field sensor is a circular loop consisting of two shielded coaxial arms which are split at the top to form a gap which is very small compared to the loop dimensions as shown in Figure 2.7. The center conductor of each coaxial arm is connected to the shield of the opposite arm, as shown at points C and D. Its configuration provides twice the equivalent area per turn and therefore increases the sensitivity. Baum [5] showed that the Moebius configuration provides twice the loop output voltage (the sensitivity of the loop is therefore increased by a factor of two). The loop time-constant (total loop winding resistance over the inductance of the loop) is increased by a factor of four and thus, the time derivative cutoff frequency f_c of the sensor is reduced by a factor of four. The Moebius loop is further more a very effective magnetic field sensing device which has good noise rejection properties (the electric field response is practically eliminated) [35].

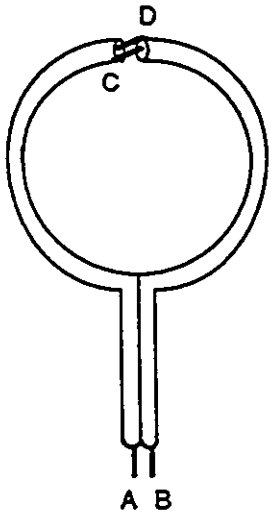

Figure 2.7: Moebius loop

Cylindrical Moebius Loop

A cylindrical Moebius loop (CML) sensor, shown in Figure 2.8[2], is described by Baum [7]. It consists of a two turn cable wired in Moebius configuration. The CML sensor has all the characteristics of the Moebius loop described in the previous section. The current flows from one twin axial cable lead to the other. The CML sensors are commonly designed to measure high frequency magnetic fields since by increasing the length of the cylinder, the inductance of the cylindrical loop decreases.

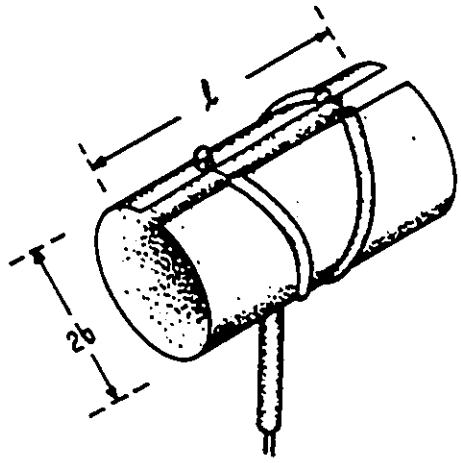

Figure 2.8: Cylindrical Moebius loop

Multi-gap Loop

The multi-gap loop (MGL) is used for high frequency magnetic field measurements [3]. It has a cylindrical geometry formed from printed circuit-board material. On the cylindrical surface there are four distinct metal areas separated

[2]This Figure is taken from Sensor and Simulation Notes Note XLII [7]

by a gap (the configuration when unfolded from the cylindrical surface is shown in Figure 2.9[3]). Both the signals from gap 1 and 3 and the signals from gaps 2 and 4 are combined together. The purpose this arrangement is to minimize the undesired response to the E-field. This kind of sensor is commonly used for far field lightning measurement.

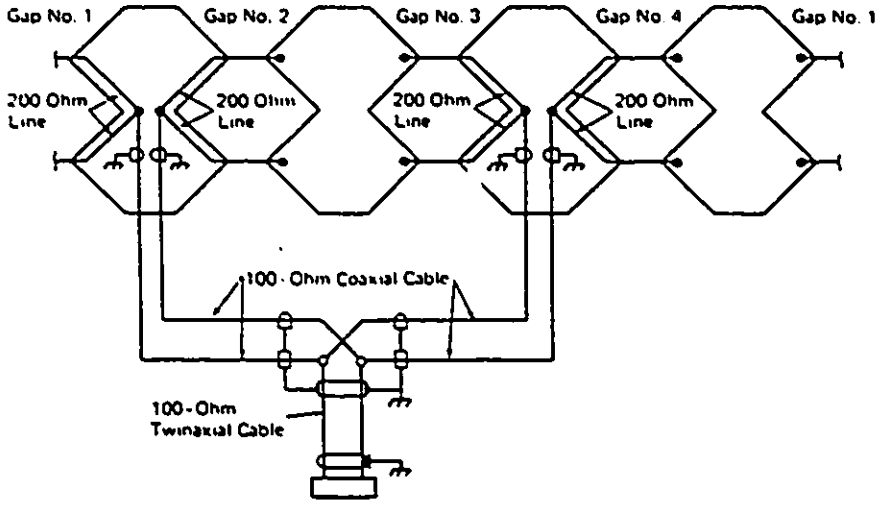

Figure 2.9: Multi-gap loop

Multi-turn Loop

The multi-turn loop (MTL) is a coil consisting of N turns and having a radius b with length l, as shown in Figure 2.10. It is commonly used in the measurement of the time varying magnetic fields such as those produced in a nuclear explosion (EMP) [16]. The MTL loop provides large equivalent area and thus a large sensitivity to the measured fields. By using many turns, the inductance

[3]This Figure is taken from Measurements of System Responses to Transient Excitations [23], pp. 272.

of the sensor is increased by N^2. Therefore, the upper frequency of the sensor is decreased by N^2 when the sensor's transfer function is proportional to the field derivative [9]. When used as a self integrating sensor, the low 3 dB roll-off frequency of the MTL loop can be made small by increasing its inductance using a ferrite core [44], [45].

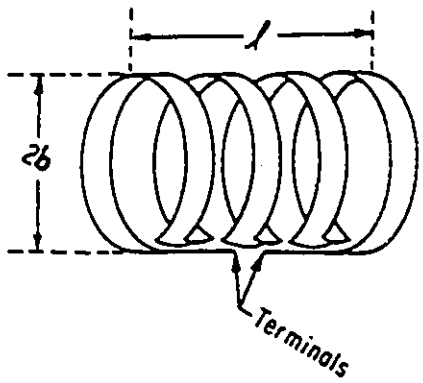

Figure 2.10: Multi-turn loop

2.2.2 Active Magnetic Field Sensors

Developments in active linear components such as transistors and integrated operational amplifiers have offered advances in the design of active magnetic field sensors. These improvements include accuracy, sensitivity, and bandwidth performance.

Several reports have been published typifying progress in this area [12], [24], [26]. MacIntyre [46] used a coil preamplifier circuit which consisted of an opera-

tional amplifier in a current follower configuration to amplify the current induced in the loop antenna. The same configuration was used by a group of researchers at the University of Ottawa [27] in a wideband magnetic field probe for transient measurements. They added a current transformer before the electronic circuit to further decrease the load resistance of the antenna.

Recently, Hauser [24] proposed in his 20 Hz-200 kHz magnetic flux probe for EMI surveys, a sensor which was based on a balanced multi-turn ferrite loop antenna and a balanced circuit which consisted of two current followers and one differential amplifier. The main advantage of using a balanced configuration in the amplification circuit was a reduction in the common mode noise.

Although, use of active linear networks for amplification in magnetic field sensors has a lot of advantages, some problems can be encountered. For instance, the active network can make up for losses in respect to signal strength by increasing background in thermal noise [18]. This problem can be overcome by using noise reduction techniques in the design stage.

2.3 Summary

In this Chapter, some of the properties of an electrically small loop antenna have been discussed. Because they are easy to design and can be made to have a low sensitivity for the electric field, they are attractive in the design of magnetic field probes. Active field probes are increasingly being used due to developments in linear integrated circuits. These advantages where reported to permit the design of

broadband magnetic field probe for the measurement of transients [27]. However, the frequency range covered by this sensor was from a few kHz to 100MHz. A question arises about the feasibility of redesigning or optimizing the previously used electrically small loop antenna to cover frequencies as low as 60 Hz. This question is addressed in the next chapter.

Chapter 3

Low Frequency Limitation of the Previous Sensor

The magnetic field probe which was developed at the University of Ottawa [27] operated in a wide frequency range from a few kHz to 100 MHz with a flat transfer function. Since many transients contain the power line frequency, it is important to extend the low frequency limit of this probe to below 60 Hz.

From a simple analysis of the equivalent circuit, given in Figure 2.3, for an electrically small loop, it was shown that the transition frequency between the derivative and flat response is given by:

$$f_t = \frac{R}{2\pi L} \tag{3.1}$$

where L represents the total inductance and R is the total resistance including the load.

A very low frequency can therefore be achieved by minimizing the total resistance and/or maximizing the inductance. This can be accomplished by

(i) minimizing the load input resistance using a current transformer for impedance transformation, (ii) increasing the loop inductance by increasing the loop number of turns N_a.

In this Chapter, the existing design will be analyzed at low frequencies to find the low frequency limitations. Following that, the impact on the high frequency performance of any changes made to achieve low frequency performance will be considered.

3.1 Description of the Sensor

The wideband magnetic sensor to be studied is depicted in Figure 3.1. This sensor consists of, (i) an electrically small loop, (ii) two current transformers (impedance transformer), (iii) a current follower (wideband transresistance amplifier).

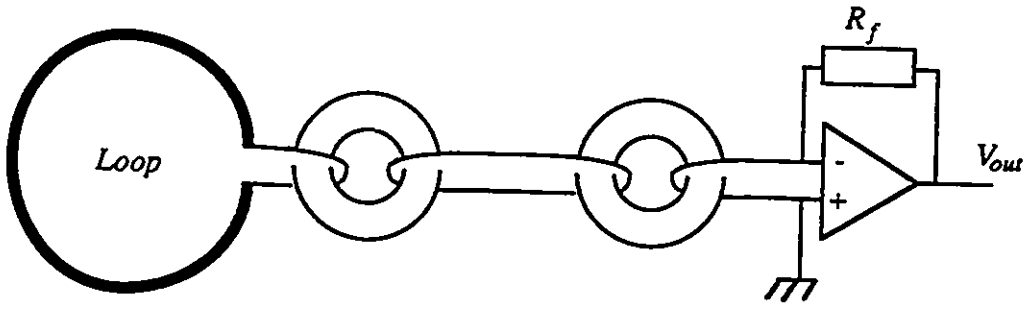

Figure 3.1: Main parts of the magnetic field sensor

The transformers and the current follower are loading the loop. To have a very low transition frequency, it is important to maintain a very small loading resistance. This is achieved through an optimization of the transformer and current amplifier design.

The primary purposes of using a transformer in this configuration are (i) impedance transformation and (ii) the attenuation of the common mode electric field interference. Transformers behave differently for different kinds of core materials used. Ferrite material with an initial permeability of 4300 has been chosen for this application since it has a uniform characteristic over a very wide frequency range [15].

The main criteria determining the suitability of the current follower in this application are:

- Input impedance of the current follower Z_{amp} which should be very small since it is a part of the loop antenna loading resistance.
- Transimpedance gain of the current amplifier V_{out}/I_i should be large.
- Bandwidth (BW) should cover the whole operating frequency range.

The magnetic field sensor of Figure 3.1 is modeled as shown in Figure 3.2. All the referred parameters in this equivalent circuit are transformed to the load side of the circuit.

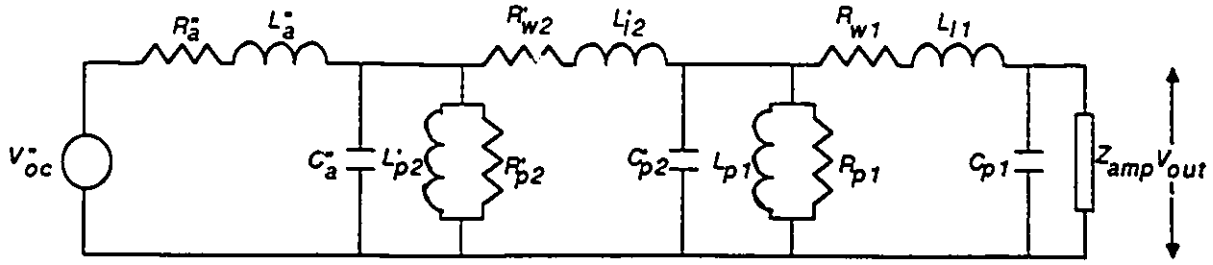

Figure 3.2: Equivalent circuit of the magnetic field sensor

where

V''_{oc} the induced open loop circuit voltage.

R''_a the winding resistance of the loop antenna.

L''_a the loop antenna inductance.

C''_a the winding capacitance of the loop antenna.

R'_{w2} total winding resistance of first stage transformer.

L'_{l2} equivalent leakage inductance of the first stage transformer.

L'_{p2} open circuit inductance of the first stage transformer.

R'_{p2} the shunt loss resistance of the first stage transformer representing the core losses.

C'_{p2} the equivalent of the primary and referred secondary self (stray) capacitance of the first stage transformer.

R_{w1} total winding resistance of second stage transformer.

L_{l1} equivalent leakage inductance of the second stage transformer.

L_{p1} open circuit inductance of the second stage transformer.

R_{p1} the shunt loss resistance of the second stage transformer representing the core losses.

C_{p1} the equivalent of the primary and referred secondary self (stray) capacitance of the second stage transformer.

Z_{amp} the equivalent input inpedance of the current follower.

N_{t1} number of secondary turns of the second stage transformer.

N_{t2} number of secondary turns of the first stage transformer.

Primed and double primed variables indicate that these values have been referred to the load side of the magnetic sensor. Primed variables are transformed once (through one transformer), double primed variables are transformed twice (through two transformers).

The inductance of the loop depends on the number of turns of the antenna, N_a, and the loop dimensions. Further details on the inductance computation is given in Appendix A.

3.2 Low Frequency Limit

When considering low frequencies, all the stray capacitances seen in Figure 3.2 behave as open circuits, they can therefore be neglected. The transformer leakage inductances are small compared to the transformer open circuit inductances. Consequently, they can also be neglected. The current follower input impedance (Z_{amp}) is assumed to be resistive and equal to R_{amp}. This assumption is justified in view of the small value of capacitance (in parallel with the resistance) and negligibly small inductance associated with leads.

Hence at low frequencies, the magnetic probe equivalent circuit of Figure 3.2 is reduced to that shown in Figure 3.3.

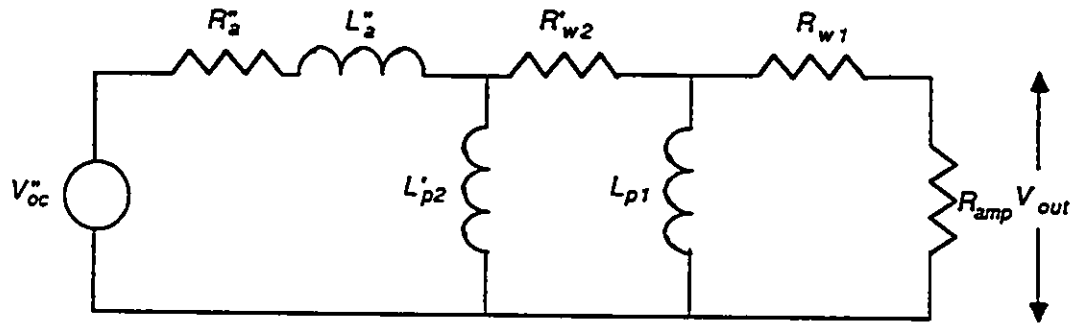

Figure 3.3: Low frequency equivalent circuit of the magnetic field sensor

The low frequency limit is determined by the highest of the three frequencies:

$$f_{t1} = \frac{R_{amp} + R_{w1}}{2\pi L_{p1}} \tag{3.2}$$

$$f_{t2} = \frac{R_{amp} + R_{w1} + R_{w2} N_{t1}^2}{2\pi L_{p2} N_{t1}^2} \tag{3.3}$$

$$f_{sens} = \frac{R_{amp} + R_{w1} + R_{w2} N_{t1}^2 + R_a (N_{t1} N_{t2})^2}{2\pi L_a (N_{t1} N_{t2})^2} \tag{3.4}$$

It can be seen that these three frequencies are basically determined by the parameters of the specific components of the circuit, with only minor contributions from other components. Therefore, the following can be designated:

f_{t1} is the low 3dB frequency of the transformer (t1).

f_{t2} is the low 3dB frequency of the transformer (t2).

f_{sens} is the low cutoff frequency of the sensor.

Equations (3.2), (3.3) and (3.4) are the low frequency design formulas for the magnetic sensor. The low roll-off frequency is the highest of f_{t1}, f_{t2} and f_{sens}. Optimizing the low frequency performance requires the optimum choice of:

- The loop geometry (the number of turns, diameter, wire diameter, shape).
- The number of transformer turns $(N_{ti})_{i=1,2}$, (for the two transformers).
- The ferrite core shape and material, since the open loop inductance of the toroids has to be maximized (equations (3.2),(3.3)).
- The current follower characteristics, since it is desirable to have an input impedance as small as possible (equations (3.2), (3.3) and (3.4)).

As will be shown later, the current follower input resistance depends on the open loop gain of the operational amplifier, the input resistance of the operational amplifier and the feedback resistor of the current follower. For the operational amplifier chosen, the input resistance is found equal to, $R_{amp} = 0.7\Omega$.

3.3 Simulation Results

The number of turns N_a, N_{t1}, and N_{t2}, as well as the ferrite core material type (characterized by its initial permeability μ_i), affect the values of R_{w1}, R_{w2}, R_a, L_{p1}, L_{p2} and L_a, which in turn determine the low frequency limit. The objective of the simulation is to see how far it is possible to lower the roll-off frequency by modifying independently the four key parameters (N_a, N_{t1}, N_{t2} and μ_i).

Three different toroids of different ferrite materials (different initial permeabilities) are considered and this just to see the effect of the ferrite core material on the two roll-off frequencies of the two transformers. The geometry of the toroids is kept the same. Three ferrite materials with initial permeabilities μ_i equal to 4300, 2000, 800 were selected.

The open circuit inductance of a toroid of an initial permeability μ_i=4300 and wound by N_t=50 turns was measured. The measured value was 6.6 10^{-3} Henries.

The open circuit inductance of any toroid having other initial permeabilities μ_i and N_t can therefore be found from:

$$L_p = \frac{6.6 \times 10^{-3}\,\mu_i}{50^2 \times 4300} N_t^2 \tag{3.5}$$

In this simulation, the loop radius "b" was kept constant equal to 3 cm (this value keeps the loop antenna electrically small for a loop number of turns N_a around 10 [27]). The equivalent input resistance of the current follower R_{amp} was assumed equal to 0.7 Ω.

A simulation was carried out to evaluate the dependance of f_{sens}, f_{t1} and f_{t2} on N_a, N_{t1}, N_{t2} and μ_i. Results of this simulation are shown in Figures 3.4 through 3.8.

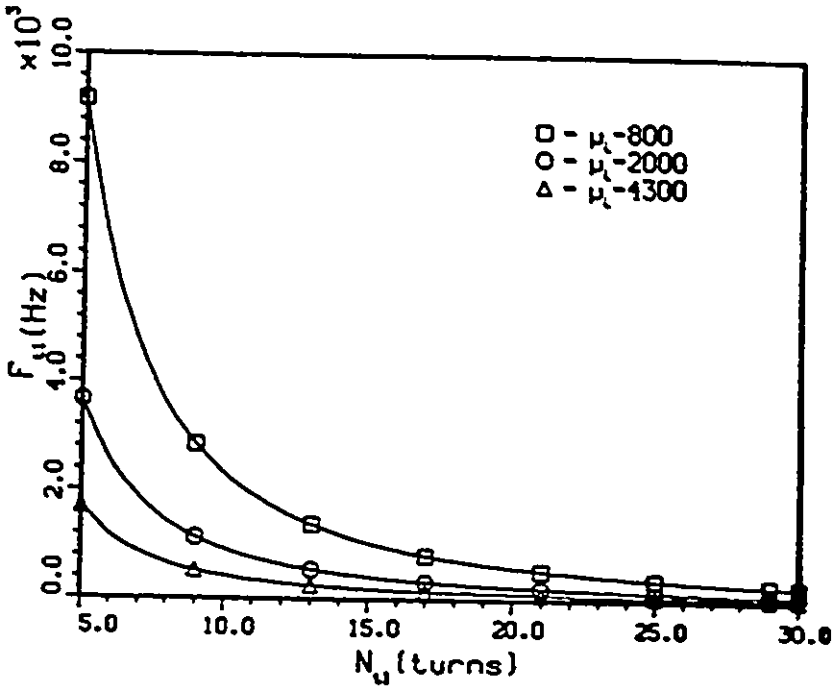

Figure 3.4: The 3dB low frequency performance of the second stage transformer vs N_{t1}

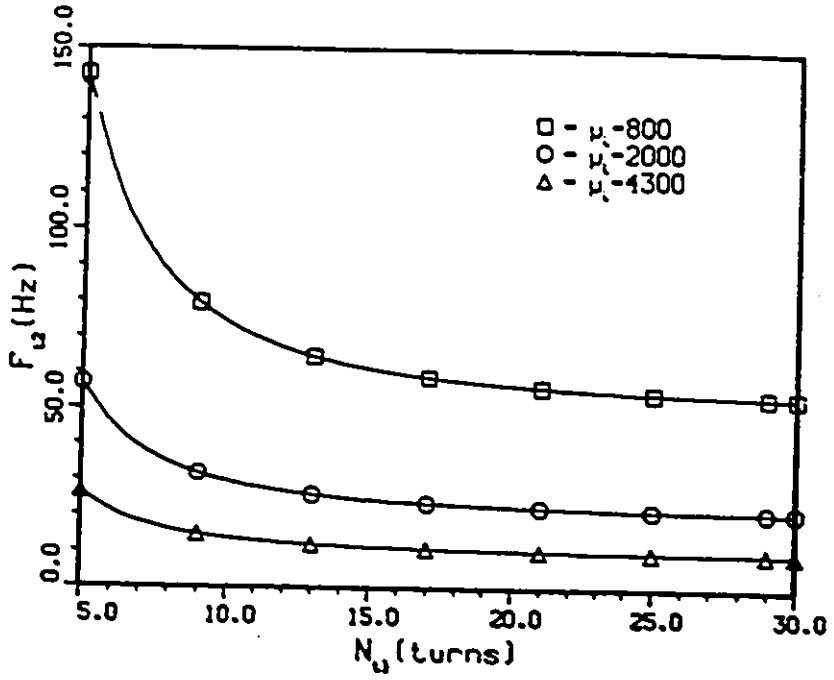

Figure 3.5: The 3dB low frequency performance of the first stage transformer vs N_{t1}

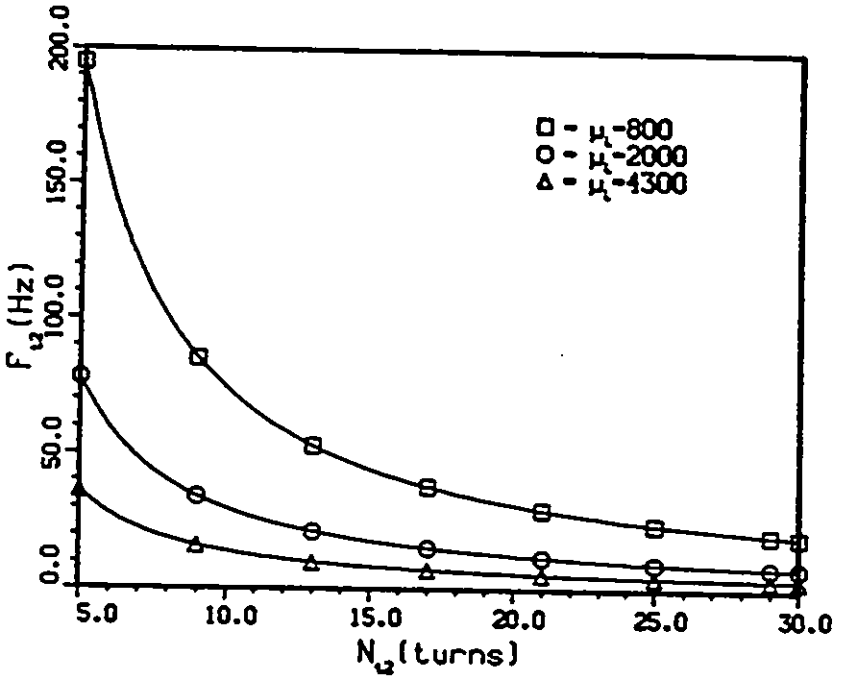

Figure 3.6: The 3dB low frequency performance of the first stage transformer vs N_{t2}

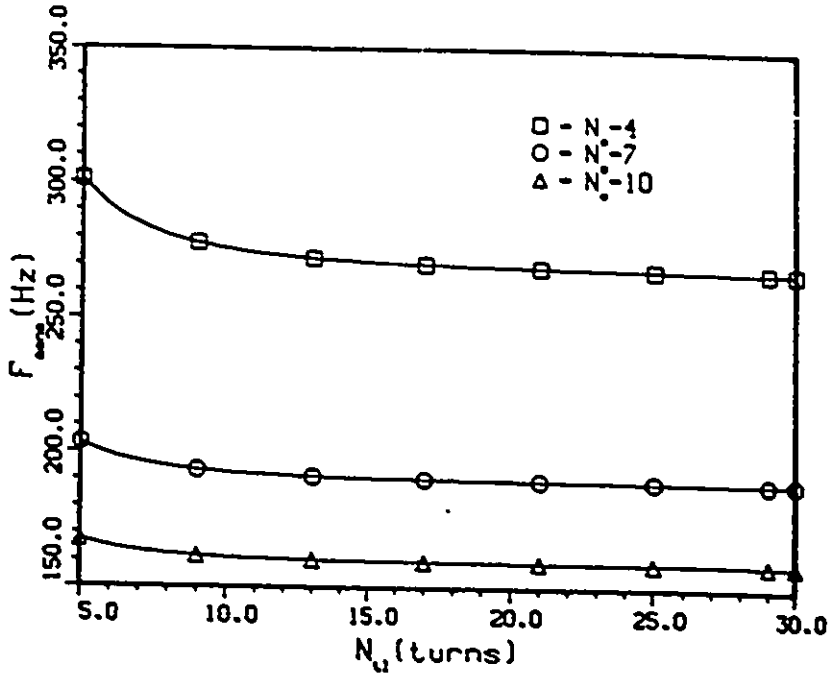

Figure 3.7: The 3dB low frequency performance of the loop vs N_{t1}

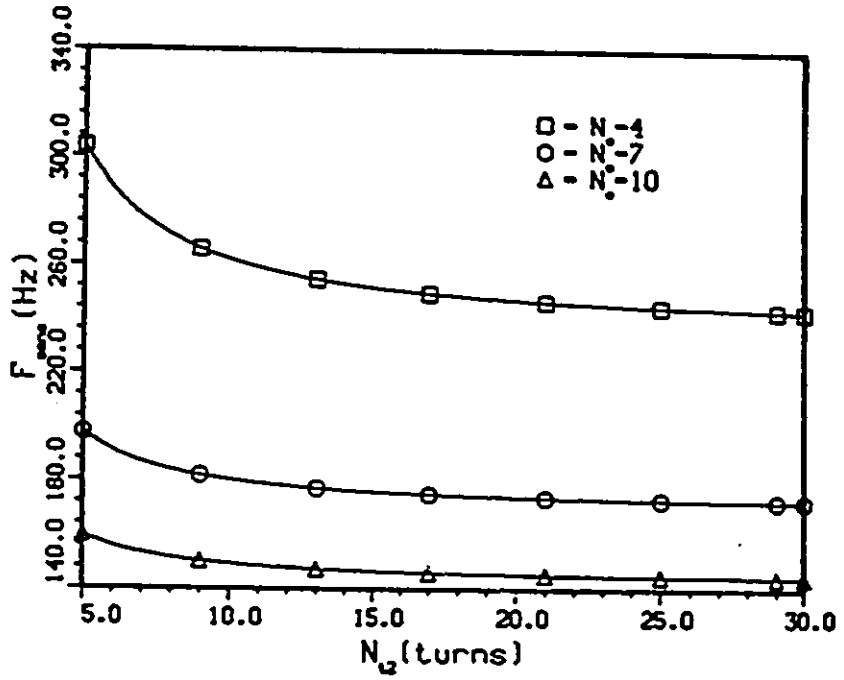

Figure 3.8: The 3dB low frequency performance of the loop vs N_{t2}

From this simulation, it can be deduced that:

- f_{t1} depends only on the secondary number of turns of the first stage transformer (N_{t1}).
- For N_{t1} greater than 15 and for μ_i greater than 4300, values of f_{t1} as small as 30 Hz can be achieved.
- f_{t2} is affected by both N_{t1} and N_{t2}. However, for N_{t1} and N_{t2} values greater than 10 turns, and for initial permeabilities μ_i greater than 2000, a lower values of f_{t2} than 30 Hz can be achieved (Figures 3.5 and 3.6).
- The number of turns of the transformers should be kept greater than or equal to 15. This result will give approximately constant values of f_{sens} as well as f_{t1} and f_{t2}.
- Ferrite core types of higher initial permeabilities have a very good performance at low frequencies. Their performance degrades at high frequencies and a trade-off should be taken depending on the operating frequency range.
- The sensor roll-off frequency f_{sens} is independent of the initial permeability of both transformers.
- f_{sens} dominates f_{t1} and f_{t2} for the transformers with a number of turns (N_{t1} and N_{t2}) greater than 15.
- A minimum value of $f_{sens} \approx 140$ Hz can be achieved for $N_a = 10$ and $N_{t1} = N_{t2} = 15$ turns.

From this simulation, it was shown that the low frequency limit is due to the antenna loop rather than the transformers (for a specified number of secondary turns). Therefore, more attention should be placed on optimizing the design of the loop antenna. This can be done, by minimizing f_{sens}, using a nonlinear constrained minimization technique which will be presented in the next section.

3.4 Sensor Optimization

A nonlinear multi-variable optimization subroutine which used NCONF (taken from the International Mathematics and Scientific Library) was used to optimize the design of the H-field sensor for a low frequency response. The details can be found in Appendix C.

To minimize f_{sens}, it is necessary to find a vector X of length N for which f_{sens} is minimum. The components of the vector X are related to some constraints which should be defined in order to optimize the loop antenna design.

The point X at which f_{sens} is calculated is a 5 dimensional vector. The components of X will be $(x_i), i = 1, ..., 5$ where :

x_1 resistance per one secondary turn of the transformer.

x_2 total length of the loop antenna wire.

x_3 resistance per unit length of the wire of the loop.

x_4 the radius of the loop (b).

x_5 the radius of the wire of the loop (a).

With N_a=10 and $N_{t1} = N_{t2} = 15$, an optimization program which minimizes f_{sens} was written. The main outcome from this program shows that a frequency as low as 120 Hz is achievable with:

x_1= 0.798 mΩ/turn.
x_2= 2.6 m.
x_3= 2.6 mΩ/turn.
x_4= 4.09 cm.
x_5= 1.43 mm.

It can be deduced using Table C.4, shown in Appendix C, that a value of f_{sens} as small as 120Hz is achievable using:

- A loop wire of gauge AWG 9.
- A loop radius of 4 cm.
- A coil of a transformer of gauge AWG 23.

3.5 Conclusion

The low frequency limit of the design described by Stuchly *et al.* [27] was evaluated in this Chapter. From this work it can be concluded that:

- If the 3 dB roll-off frequency of below 60 Hz is to be achieved with an air loop antenna, it will lead to a multi-turn loop with big radius (greater than 3 cm) and large number of turns (greater than 30). This in turn will lead

to a low 3 dB roll-off upper frequency because of the long wire and / or the inter-winding capacitance.

- Alternatively, a very thick wire could be used for the multi-turn loop (low resistance per unit length). But, this leads also to a bulky and heavy sensor. Besides that, the problem of inter-winding capacitance will not be eliminated.

- An alternative solution is to consider a use of a ferrite core in the loop [1],[11] which would increase the inductance, but practically would not affect the resistance.

Chapter 4

Design of a Magnetic Field Sensor

The H-field sensor described by Hauser [24] has the advantage of the very low 3 dB cutoff frequency, however, its high corner frequency is limited to 200KHz which is small for wideband applications whereas the H-field sensor described by Stuchly, *et al.* [27], has the advantage of a wide operating frequency range. In this Chapter, the two advantages of these two probes were taken into consideration to develop a new design of a magnetic field sensor with the features required of this thesis.

4.1 General Overview of the Design

Calculations described in Chapter 3 showed the limitations of an air loop antenna in achieving the desired low roll-off frequency. An increase in the loop inductance can be accomplished by using a multi-turn ferrite rod loop antenna. The ferrite material can be chosen such that its effective permeability is high enough to get high inductance and thus a low loop transition frequency (eq. 3.4).

The loop antenna load resistance (R_{amp}) can be lowered by choosing an operational amplifier with high open loop gain (A_0). Such amplifiers do not usually operate at frequencies above tens of MHz, which is adequate for this design. This can lead to the elimination of at least one of the transformers present in the previous design.

For noise reduction, it is advantageous to use a balanced configuration. This can be done by loading the multi-turn ferrite loop antenna by a center-tapped transformer and an instrumentation amplifier as that described by Hauser [24].

4.2 Loop Antenna Design

To obtain a low 3 dB roll-off frequency a high inductance is needed while maintaining a low resistance. This could be achieved by using a ferrite rod cored antenna. The important considerations when selecting the ferrite material and designing the antenna are size and material losses. The problem can be defined as obtaining a given value of inductance in the smallest volume occupied by the wire while keeping the total effective resistance below a specified value. The loop resistance depends not only on ohmic losses in the coil conductor but also on loss mechanisms existing in the magnetic core material. Ferrite core losses are classified as follows, (i) eddy current losses, (ii) hysteresis losses, and (iii) residual losses [34]. At low frequencies (below a few megahertz), for high permeability ferrites, eddy currents are insignificant; also hysteresis losses are negligibly small [15]. Therefore, the magnetic losses can be neglected. The absence of eddy currents in the ferrite

allows the high permeability of the material to be effective in producing a large concentration of magnetic flux in the rod.

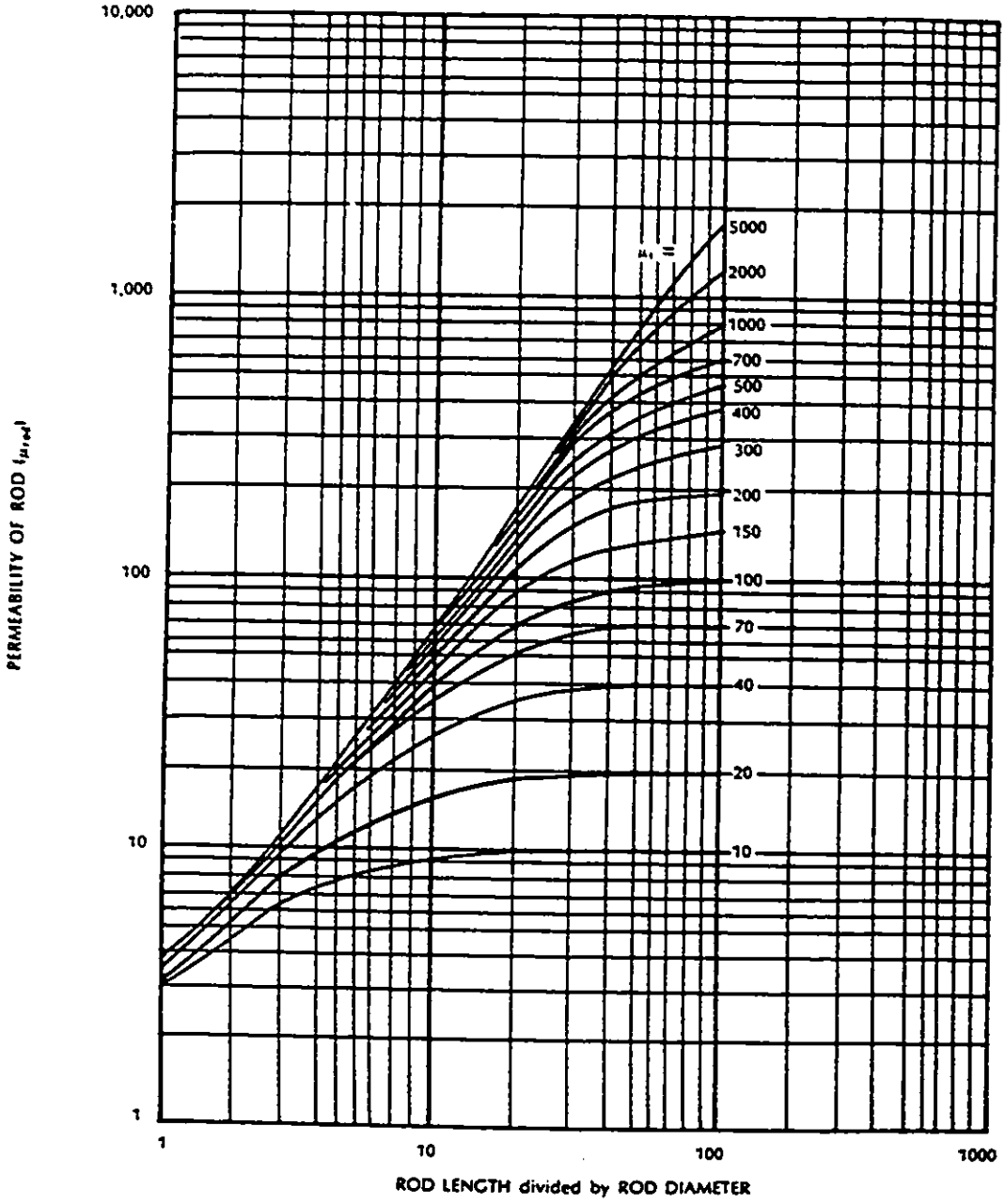

Figure 4.1: Relative permeability of a ferrite rod vs the length to diameter ratio for various material permeabilities

The effective permeability of a ferrite rod is a function of its length to diameter ratio as well as the material permeability. Curves shown in Figure 4.1 [17] indicate that the effective permeability of a rod can be substantially smaller than the initial material permeability. It also illustrates that the effective permeability of a rod is influenced by its dimensions and geometry more than by its material permeability.

To obtain high effective permeabilities, the ratio of length to diameter should be large according to Figure 4.1. However, in practice, the length of the loop antenna should be reasonably small in order to not excessively perturb the measured field.

In order to evaluate how reliable is the data on effective permeabilities provided by the manufacturer (Figure 4.1), the effective permeability was evaluated by direct measurements. The effective permeability of the rod material can be evaluated by measuring the inductance of the loop antenna with and without a ferrite rod core. The effective permeability of the coil can be expressed as:

$$\mu_c = \frac{L_a}{L_w} \tag{4.1}$$

with:

$$\mu_c = \mu_{rod}\, F_L \tag{4.2}$$

where,

L_a inductance of the ferrite core antenna.

L_w inductance of the air core antenna.

F_L empirical factor which can be determined by an average of experimental results [17].

μ_{rod} apparent permeability of the rod material.

A measurement of a 20 turn loop antenna inductance (solenoid) was performed using a network analyzer, HP 3577A, for each kind of material. The results are summarized in Table 4.1.

Table 4.1: Evaluation of the measured and calculated loop inductance

Core Type Material	Length (cm)	Rod Diameter (cm)	Initial Permeability	Measured Inductance (μH)	Calculated Inductance (μH)	μ_e
#61	19	1.27	125	17.8	18.3	27.7
#33	19	1.27	800	28.5	29.4	44.4
#33	12	1.27	800	19.7	20.3	30.7
Air	-	1.27	-	0.642	0.663	-

It can be seen from Table 4.1 that it is advantageous to use a ferrite rod made of material #33, of a length of 19 cm, since it gives a high effective rod permeability and therefore the lowest 3 dB low roll-off frequency. Unfortunately, this will result in a relatively long antenna which may perturb the EM field. To avoid this problem, the rod material of length 12 cm is chosen for this application.

The difference between the apparent permeability (μ_{rod} which is deduced from Figure 4.1) and the effective permeability (μ_e from Table 4.1) of a given rod material can be attributed to the fact that, even though the flux density in the rod is increased over the flux density when the rod is absent, its presence does not

increase the inductance of such a coil by the same factor since it furnishes only a part of the magnetic circuit of the coil [15].

Figure 4.2 shows the effect of the number of turns (N_a) of the loop on its cut-off frequency (f_a), when the loop is short circuited ($R_L = 0$). A wire of gauge AWG 9 is used in this case ($b = 0.63$ cm). The decrease in the roll-off frequency is very small for the number of turns greater than 20. Therefore, 20 turns are selected for the design.

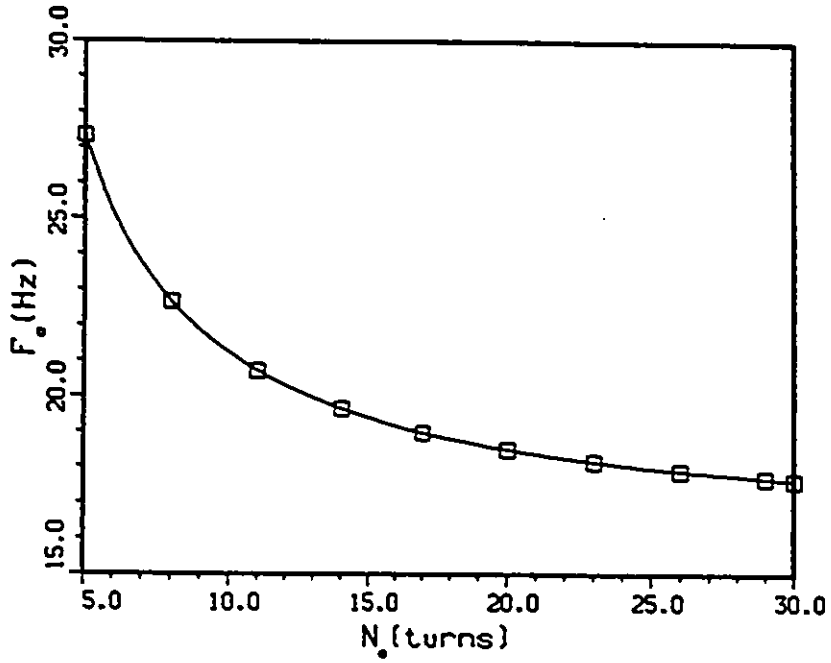

Figure 4.2: Selection of the loop number of turns

4.3 Transformer Design

For convenience, the term "analog transformer" is used in this section to describe a transformer designed to carry a wide-band, low power harmonic sig-

nal and the term "pulse transformer" is used for a transformer which carries a pulsed signal. Since a pulse train has a definite frequency spectrum, the design considerations for the two types of transformers are similar. However, the analog transformer is specified in the frequency domain, whereas the pulse transformer is specified in the time domain.

The difference between analog and pulse transformers resides in the fact that the first one is usually required to transmit a specified bandwidth over which the attenuation should not exceed a specified value, whereas the second is required to transmit a given pulse shape with a specified limit on the shape distortion. Generally, a transformer design that gives a good, wide frequency response will also give a good transient response.

Our objective in this section is to design a balanced wide-band transformer with the following characteristics:

- A very low 3 dB roll-off frequency.
- Constant amplitude and phase over a broadband frequency range.
- Good performance in both the time and frequency domains.

From the lumped equivalent circuit of the transformer shown in Appendix B, Figure B.2, it can be deduced that the shunt inductance, L_p, is responsible for the low frequency roll-off in the analog transformer since its reactance progressively shunts the circuit as the signal frequency decreases. In the case of the pulse transformer, the shunted inductance causes the top of the pulse to droop because,

during the pulse, the magnetizing current in L_p increases almost linearly with time causing a voltage drop across the source resistance.

The winding resistance R_w is also important in low frequency analysis; however, R_w is the main cause of the mid-band attenuation in low frequency analog transformers. In a pulse transformer, it is usually reflected as the attenuation of the output pulse but, very often, has no effect on the pulse distortion.

In summary, it can be said that the shunt inductance as well as the winding resistance have significant effects on the low frequency performance of the transformer.

The high frequency roll-off of the transfer function of the transformer may be due to either the increasing series reactance of the leakage inductance L_l or the decreasing shunt reactance of the self capacitance C_w, or a combination of both, as the frequency increases. In the pulse transformer, the leakage inductance, self capacitance and source or load resistance, affect the delay as well as the rise and fall times of the output pulse.

The performance of the toroidal core depends on the effective permeability which in turn depends on the initial permeability as discussed earlier. The shunt or open loop inductance is the circuit element that is associated with the magnetizing current. Ideally this inductance should be as large as possible so that the magnetizing current will be small. This can be accomplished by using enough turns in the winding. However, if the core is physically too small, this will lead to an increase in the winding resistance R_w (because of the thin wire), causing a

high mid-band or pulse attenuation.

The ratio of the winding resistance R_w to the shunt inductance can be expressed by [34]:

$$\frac{R_w}{L_p} = (\frac{l_w l_c}{A_w A_c})\frac{1}{\mu_e} \tag{4.3}$$

where

l_w mean turn length of the winding

l_c effective length of the magnetic circuit.

A_w cross sectional area of the winding.

A_c effective cross sectional area of the magnetic circuit.

μ_e effective permeability of the magnetic circuit.

Therefore, for a given toroid, R_w is proportional to L_p since the ratio R_w/L_p is independent of the number of turns. In order to get small ratios of R_w/L_p, it is important to select ferrites of high permeabilities.

The high frequency or transient response depend on the leakage inductance which is equal to [15], [34]:

$$L_l = \mu_0 \, N^2 \, l_w \, \frac{b_w}{3 \, h_w} \tag{4.4}$$

The ratio of the open circuit to the leakage inductances is given by the following equation [34]:

$$\frac{L_p}{L_l} = \frac{3\mu_0 b_w}{l_w \, h_w \, C_1} \tag{4.5}$$

where

h_w winding height.

b_w winding width.

l_w mean turn length.

C_1 core factor.

$$C_1 = \frac{l_e}{A_e} \tag{4.6}$$

In order to obtain large L_p/L_l, a multi-turn winding is desirable since it increases b_w (equation 4.4). However, this is contradictory to the requirement of an optimum geometry for minimum R_w/L_p. A trade-off may be sought by increasing b_w and decreasing h_w by an amount that does not increase R_w/L_p beyond a few percent.

The desired low frequency performance of the transformer is ensured by selecting a ferrite toroid material with a high effective permeability and a large value of core factor C_1.

Ferrite material manufacturers specify in the data sheets the effective length and the cross sectional area of the magnetic circuit. The inductance per turn A_l is also specified.

The inductance L of N turns is:

$$L = A_L N^2 \tag{4.7}$$

and

$$A_L = \frac{\mu_0 \mu_e}{C_1} \tag{4.8}$$

At high frequencies, the leakage inductance is reduced by; (i) selecting a reasonably number of turns (but such that the ratio R_w/L_p will not exceed a specified value imposed by the low frequency criteria) (ii) selecting an optimum core geometry (to fulfill the high frequency criteria) and (iii) reducing the resonating capacitance by providing uniform spacing between the windings.

In this design, a Fair-Rite toroid made of material 75 has been selected. Its part number is 5975004901. Its characteristics are gathered in Table 4.2. A center tapped transformer was made using 8 turns in each secondary side of wire AWG 24.

Table 4.2: Characteristics of the toroid selected

$A_e(mm^2)$	20.3
l_e (mm)	39.4
A_L (nH/turn)	3240
d_1 (mm)	16
d_2 (mm)	9.6
h_w (mm)	6.35
l_w (mm)	19.1
C_1 (mm^{-1})	1.94
μ_e	5000

4.4 Electronic Circuit Design

The output current of the transformer is processed to be converted to an output voltage by an instrumentation amplifier. The circuit, as illustrated in Figure 4.3, shows that the two front ends are current followers and the output stage is a differential amplifier.

The main parameters determining the suitability of the current follower in this application are input impedance Z_{amp}, gain V_c/I_i and bandwidth. These characteristics are closely interrelated and are largely determined by the operational amplifiers selected. For the differential amplifier, the gain-bandwidth product as well as the offset drift parameters are of great importance. In this section, some design criteria are given which justify the circuit architecture and the operational amplifier selection.

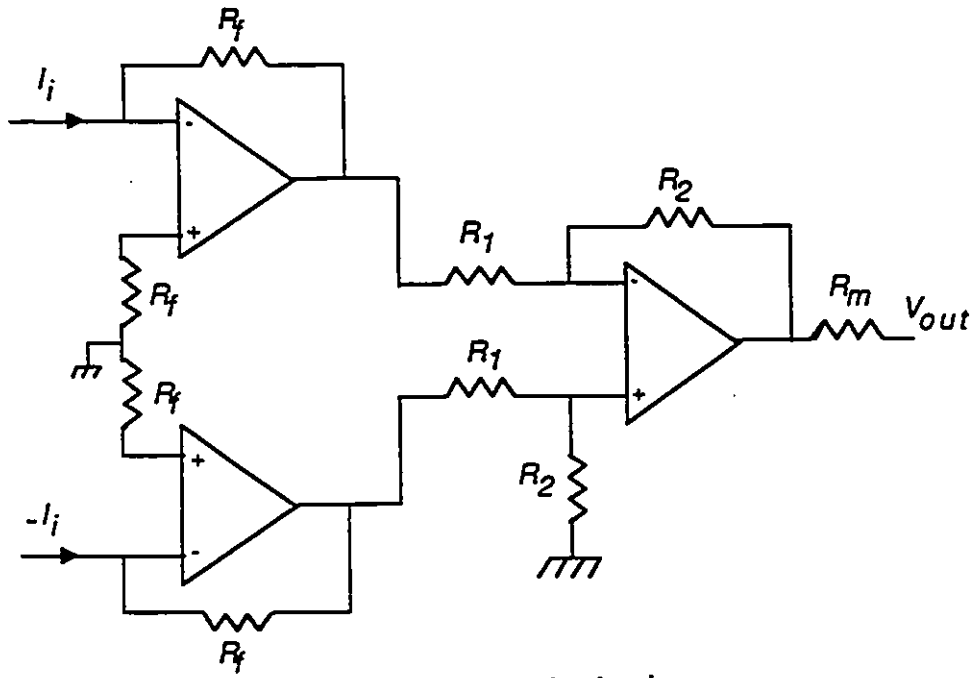

Figure 4.3: Electronic circuit

4.4.1 Current Amplifier Design Criteria

The current follower, as depicted in Figure 4.4, is convenient for this application in the sense that it approaches the ideal current meter. There is essentially no voltage drop across the measuring circuit since with sufficiently large open loop gain, the input impedance becomes very small [2]. Indeed, this configuration usually provides a stabilized transfer function (V_c/I_i) that has the dimensions of impedance. Such a circuit is often called a current to voltage converter or transimpedance amplifier.

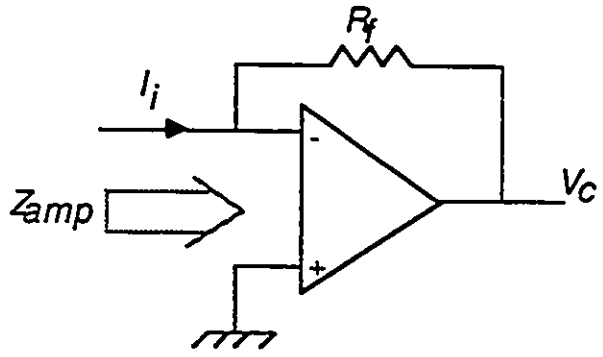

Figure 4.4: Current amplifier configuration

The input impedance of the current amplifier loading the loop antenna is a very important design parameter which affects the low frequency performance of the magnetic field sensor. Assuming that the operational amplifier has one pole frequency ω_0, such that the gain can be expressed as $A(s) = \frac{A_0}{1+s/\omega_0}$, then the amplifier input impedance can be calculated by one of the following formulas:

- For $\omega \leq \omega_0$:

$$|Z_{amp}| \approx R_{in}||\frac{R_f}{1+A_0} \tag{4.9}$$

- For $\omega \geq \omega_0$:

$$|Z_{amp}| \approx |R_{in}||R_f\frac{1+\frac{s}{\omega_0}}{A_0}| \tag{4.10}$$

- For $\frac{s}{\omega_0} \gg A_0$:

$$|Z_{amp}| \approx R_{in}||R_f \tag{4.11}$$

where

s complex angular frequency.

A_0 low frequency open loop gain.

R_{in} operational amplifier input impedance.

R_f current amplifier feedback resistance.

A_0 and R_{in} are given in the operational amplifier data sheets.

The output voltage of the current amplifier is given by [2]:

$$V_c = -R_f(I_i + v_{os}\frac{R_f + R_s}{R_s R_f} + i_b) \tag{4.12}$$

where

V_c current amplifier output voltage.

I_i current amplifier input current.

R_f feedback resistance.

R_s current source resistance.

e_{os} input offset voltage.

i_b input bias current.

Therefore, the current amplifiers should have the following features: (i) current noise and bias current drift as small as possible, (ii) high operational amplifier open loop gain A_0, and (iii) high slew rate and fast settling time for transient response considerations.

4.4.2 Differential Amplifier Design Criteria

The purpose of using a differential amplifier is to get an output proportional to the difference between the two input signals. Its circuit configuration, as illustrated in Figure 4.5, is especially useful when each of the input signal is contaminated by common mode noise, or a noise source which is the same or common to both input signals. The circuit has two inputs and one output, and ideally, the output from this amplifier depends only on the difference between the inputs.

For the analysis purposes, the input signals to this amplifier have been separated into two components: the differential and common mode components. Assuming that our circuit is perfectly balanced and that $v_{d1} = -v_d/2$ and $v_{d2}=v_d/2$

represent the signals whose difference v_d should be amplified and that v_{cm} represent a common mode noise signal which is assumed in equal amounts at both terminals of the amplifier. The purpose of using the differential amplifier is to amplify the differential portion of the input signal while rejecting the common mode component. The ability of a specific amplifier to accomplish this task is indicated by its common mode rejection ratio which is defined as [36]:

$$CMRR = \frac{A_d}{A_{cm}} \tag{4.13}$$

where,

$$A_d = \frac{v_0}{v_{d2} - v_{d1}} = \frac{v_0}{v_d} \tag{4.14}$$

and,

$$A_{cm} = \frac{v_0}{v_{cm}} \tag{4.15}$$

A_d and A_{cm} represent respectively the differential and common mode gain of the differential amplifier.

The differential gain of the operational amplifier may be found by setting v_{cm}=0 :

$$A_d = \frac{v_0}{v_d} = \frac{R_2}{R_1} \tag{4.16}$$

The common mode gain of the differential circuit can be found by letting the two sources $v_d/2$ equal zero:

$$A_{cm} = (1 + \frac{R_2}{R_1})\frac{R_2/R_1}{1 + R_2/R_1} - \frac{R_2}{R_1} \tag{4.17}$$

It is apparent that $A_{cm}=0$ if the resistors are perfectly balanced. However, in practice, it is likely impossible to get a $CMRR$ equal to infinity, because two resistors can never be perfectly identical. In reality, resistors are specified to some tolerances and it can be shown that [36]:

$$CMRR = \frac{1 + R_2/R_1}{4T_o} \tag{4.18}$$

where T_o is the resistor tolerance.

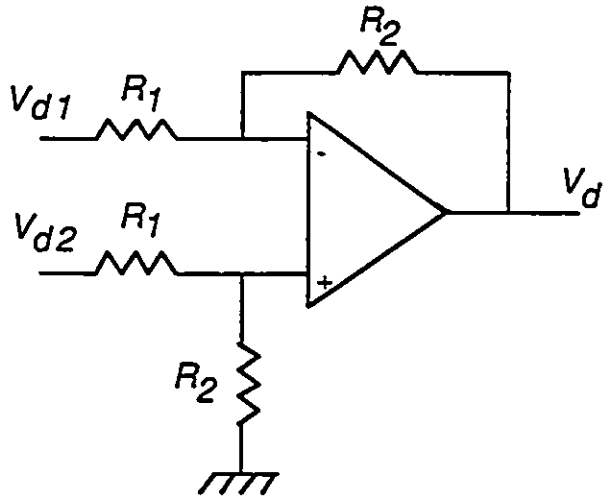

Figure 4.5: Differential amplifier configuration

In summary, in this application, the differential amplifier circuit requires precise resistor matching to achieve a high common-mode rejection ratio. The slew rate and settling time are the specifications which determine the transient response. The restrictions on the full power response and slew rate should be observed in order to limit distortions and unexpected dc offsets at the output of the amplifier.

4.4.3 Operational Amplifier Selection

Following the criteria outlined, the OP37 precision operational amplifier has been selected for the current amplifiers. It has the advantage of a high open loop gain (120 dB), small input bias current (40 nA) and low drift offset voltage ($0.6\mu V/°C$), and a wide gain-bandwidth product (63 MHz). A feedback capacitor is added to the current amplifier architecture to compensate, in part, the stray capacitances due to the antenna and current transformer.

For the differential amplifier, the low distortion precision wide bandwidth AD961S has been selected. It offers a fast settling, a very high slew rate and a large gain-bandwidth product of 160 MHz.

The chip resistors that have been chosen in this configuration are within 1% tolerance which ensure a high $CMRR$ in the differential amplifier ($\approx$ 50 dB).

The layout has been optimized for high frequency performance (using Hi-Wire software). Surface mount technology and chip resistors and capacitors have been used. It is this circuit which has been used in the subsequent measurements.

Chapter 5

Simulation and Measurements

In order to evaluate the performance of a magnetic field sensor consisting of a multi-turn ferrite-cored loop antenna, a center tapped current transformer and a balanced current and differential amplifier, AC and transient analysis were performed using **Hspice**[1] simulation. Test measurements in both the time and frequency domains were made to characterize the sensor.

5.1 Hspice Simulation of the Magnetic Field Sensor

Hspice software for electric circuit simulation has been used to analyse the behavior of the magnetic field sensor in the time and frequency domains [29]. The choice of this software for this application was made because of the variety of options it offers. Furthermore, Hspice furnishes an internal operational amplifier

[1] Hspice is a simulation program more commonly used for computer aided design of integrated circuits, Meta-Software Inc. [29].

macro-model which can be used directly in this simulation. Additionally, there is the possibility of using algebraic expressions which facilitates AC and transient analyses (bandwidth, rise/fall time etc..). In this section, the Hspice model of the magnetic field sensor is derived, simulation is then performed of AC and transient analysis of the probe.

5.1.1 Hspice Magnetic Field Sensor Model

The magnetic field sensor has been modeled as shown in Figure 5.1.

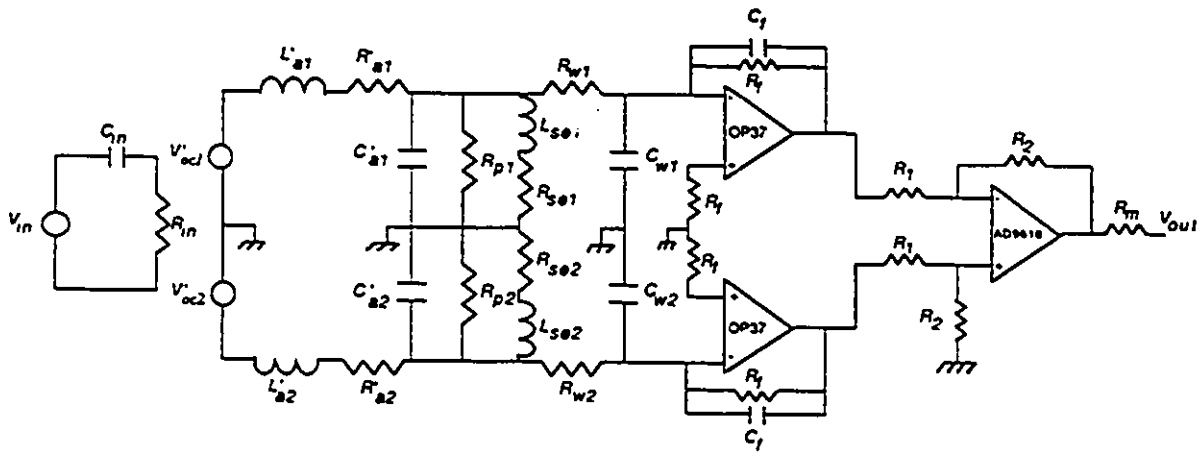

Figure 5.1: Hspice magnetic field sensor model

where,

V'_{oc} The induced open loop voltage transformed to the secondary side of the transformer.

R'_a The equivalent winding resistance of the loop antenna trans-

formed to the secondary side of the transformer.

L_a' The inductance of the loop antenna transformed to the secondary side of the transformer.

R_p' The dielectric loss resistance due to the rod material transformed to the secondary side of the transformer.

C_a' The equivalent stray capacitance of the rod antenna transformed to the secondary side of the transformer.

R_{se} The series loss resistance of the transformer.

L_{se} The open loop series inductance of the transformer.

R_w The equivalent winding resistance transformed to the secondary of the transformer.

C_w the equivalent stray capacitance of the transformer.

The leakage inductance of the transformer is omitted from the equivalent circuit since a perfect coupling between the primary and secondary windings is assumed. For high permittivity toroids, this assumption is justified.

The induced open voltage source, given by equation (2.3), is proportional to the time derivative of the magnetic field. It can be modeled by an R-C circuit and a voltage controlled voltage source of gain A which reflects the magnitude of the magnetic field received by the antenna. The gain A can be expressed as;

$$A = \frac{\mu_0 \, \mu_c \, A_a \, H_{TEM} \, N_t}{R_{in} \, C_{in}} \tag{5.1}$$

where

μ_0 air permeability.

μ_e effective permeability of the antenna.

A_a effective area of the loop antenna.

H_{TEM} magnitude of the magnetic field intensity in the TEM cell.

N_t turn ratio of the transformer.

Equivalent circuit parameters have been measured as derived in Appendix D. All measurements have been made in the experimental system described in section 5.2. The measured gain is $A \approx 6\ 10^6$. Other parameters are summarized in Table 5.1. These parameters have been obtained from Figures D.1 and D.2 (Appendix D). These Figures show Bode (impedance) diagrams for the loop antenna, and the secondary of the transformer, respectively. On each diagram five point have been identified and used in calculating the equivalent circuit parameters, namely:

- The 3 dB low roll-off frequency (f_{3dB}) indicated when the phase $\phi = 45^o$.
- The mid-band frequency impedance when it is purely inductive, i.e $\phi = 90^o$ (Z at $f = f_m$).
- The resonant frequency (f_0).
- The frequency f_1, 3 dB below f_0, when $\phi = 45^o$.
- The frequency f_2, 3 dB below f_0, when $\phi = -45^o$.

The identified parameters of the loop antenna and transformer are gathered in Table 5.1.

Table 5.1: Magnetic field sensor parameters identification

Parameters	*Loop Antenna*	*Transformer*	
		side 1	Side 2
f_{3dB} (Hz)	16	25.6	22.6
Z at $f = f_m$(dB)	21.55	26.4	21.44
f_1 (MHz)	14.9	0.82	0.82
f_2 (MHz)	27.9	17.2	17.9
f_0 (MHz)	19	4	4.15
$R_a(m\Omega)$	2	-	-
$L_a(\mu H)$	19.7	-	-
$C_a(pF)$	3.55	-	-
$R_p(K\Omega)$	3.4	-	-
$L_{se}(\mu H)$	-	148.7	187.7
$R_{se}(K\Omega)$	-	0.91	1.18
$R_w(m\Omega)$	-	23.9	26.7
$C_w(pF)$	-	10.6	7.8

The electronic circuit model can be readily derived since the Hspice simulator offers an internal operational amplifier model which generates a subcircuit macro-model in the output listing. In this application, an operational amplifier macro-model is created when its model parameters are specified in the simulation program.

5.1.2 Hspice AC Analysis of the Sensor

Figure 5.2 shows the AC simulation of the sensor. It indicates constant amplitude from 27 Hz to 27 MHz (± 3 dB). The phase is constant from 27 Hz to

8.3 MHz (±45°). The difference in the bandwidth for the magnitude and phase is due to the tune-out capacitances used in parallel with the feedback resistors in the two current followers.

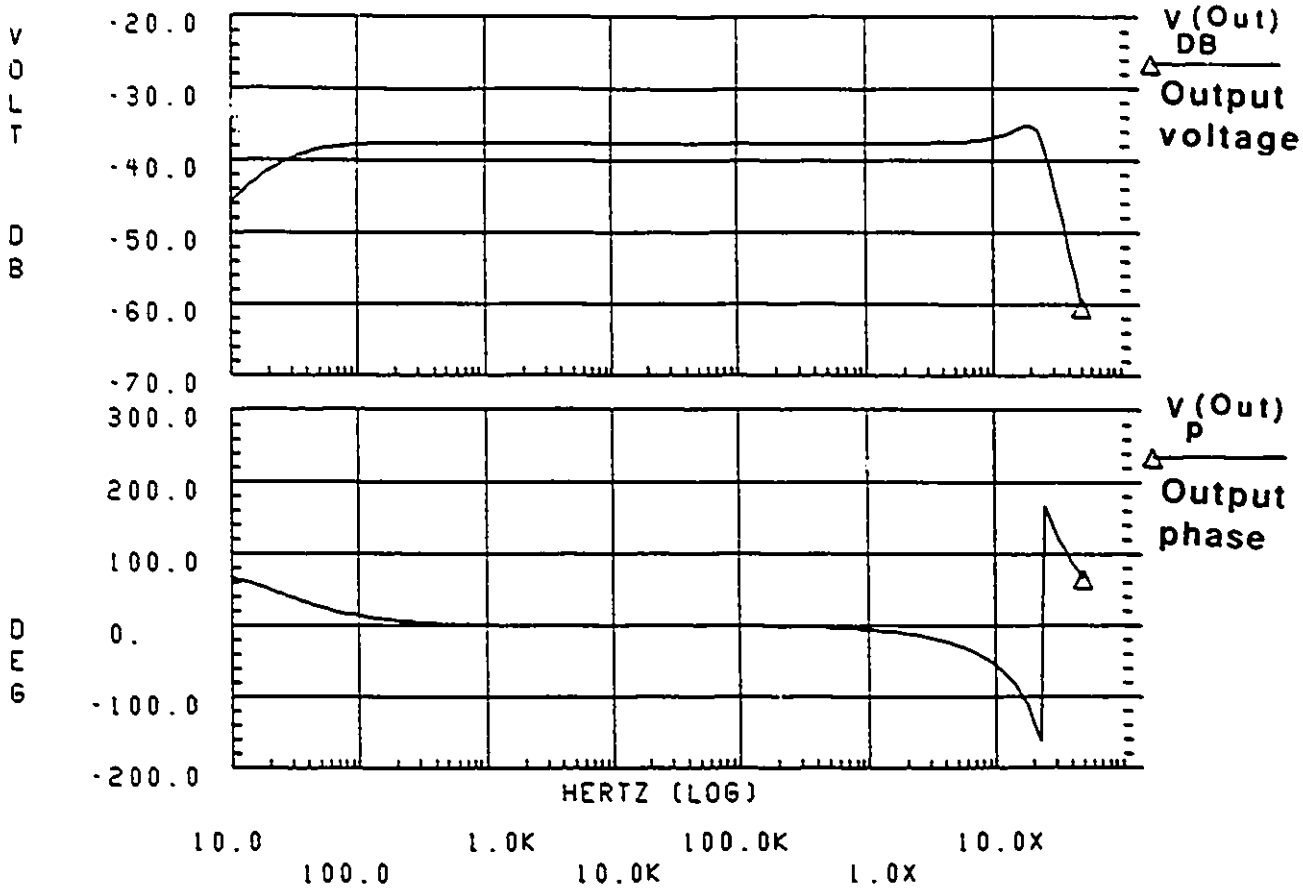

Figure 5.2: Hspice AC simulation

5.1.3 Hspice Transient Analysis of the Sensor

Figure 5.3 shows the impulse response of the sensor. The ripples in the output voltage are due to the resonant frequency which is around 27 MHz (see Figure 5.2).

A number of simulations were performed for different rise and fall times of the input pulse. The rise and fall time of the output pulse were calculated from 10% to

90% of the maximum magnitude of the output pulse. The results are summarized in Table 5.2 (the difference between the rise and fall times of the output pulse is due to the mismatching between the the components of the transformer referred to each side of the balanced model of Figure 5.1).

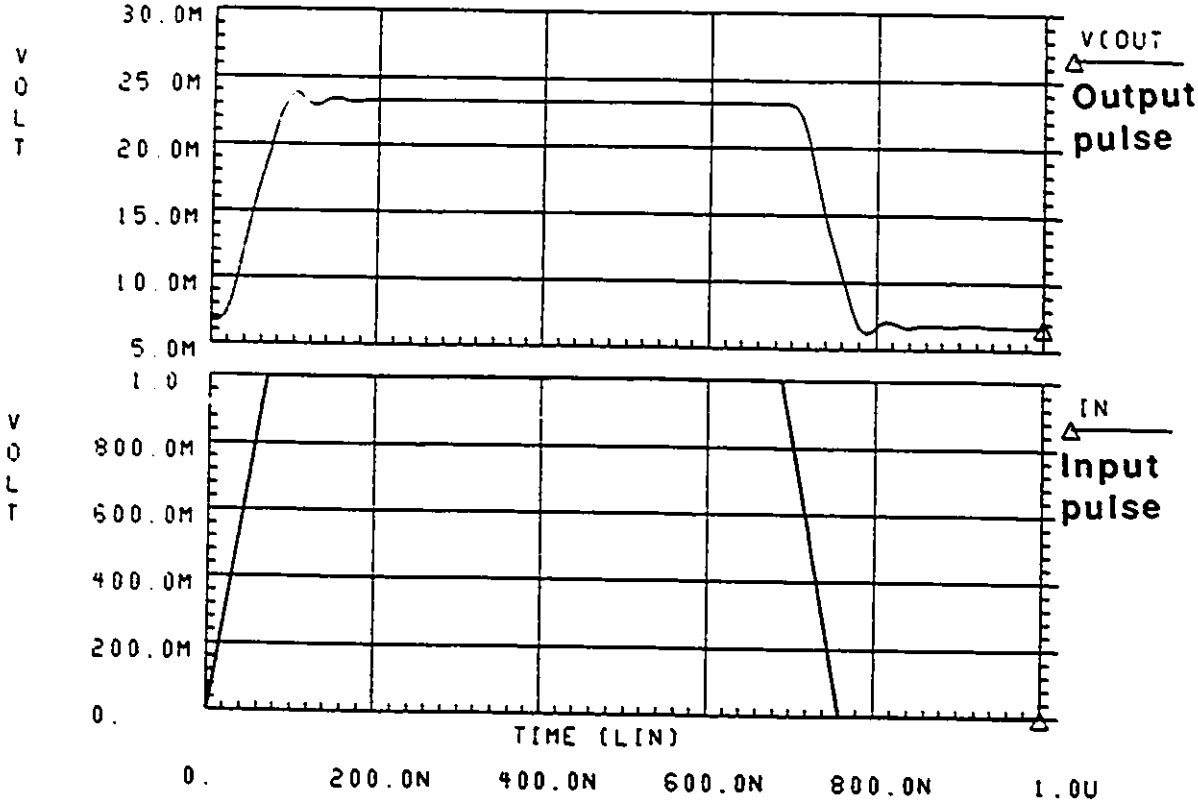

Figure 5.3: Hspice pulse response of the sensor

Table 5.2: Calculated rise and fall times

Input pulse		*Output Pulse*	
Rise time (ns)	Fall time (ns)	Rise time (ns)	Fall time (ns)
64	64	78.3	69.7
40	40	52.9	44.6
24	24	40.6	29.6
16	16	34.4	27.6
8	8	28.4	21

5.2 Measurements

No attempt has been made to simulate some features of the magnetic field sensor (e.g electric field interference or dynamic range). For full performance analysis of the sensor, measurements in both the time and frequency domains have been performed.

The following equipment was used in the experiments:

- **HP 3577A NETWORK ANALYZER** 3 input, dual trace, synthesized, 5 Hz-200 MHz programmable Network Analyzer (NA) [19].
- **35676A Reflection / Transmission test kit**, an integral part of the HP 3577A network analyzer.
- **HP Graphics Plotter**, model 7470 A, compatible with the network analyzer.
- **TEM Cell** operating from few Hz to 1 GHz [30], [31], [43].
- **Tektronix 11802 Digital Sampling Oscilloscope.**,

5.2.1 Frequency Domain

The performance of the sensor in the frequency domain can be analyzed by measuring its transfer function T (forward gain and phase).

Figure 5.4 shows the block diagram of the experimental arrangement (nodes

"C_1, 1" and "C_2, 3" are connected). The probe is inserted vertically as depicted in Figure 5.4. The probe should be small compared with the dimensions of the TEM cell so that it is reasonable to neglect the higher order modes exited by the discontinuity produced by the probe [38]. The TEM cell is chosen such that, the TEM cell cutoff frequency (1 GHz for the TEM cell used) is higher than the highest test frequency. The TEM cell cutoff frequency is defined as the frequency at which higher order modes begin to propagate [30]. Below the cut-off frequency, and when the cell is terminated with its characteristic impedance (50Ω), a TEM field exists within the cell structure. This TEM field approximates a plane wave, and, consequently a well defined and uniform field exists over the central portion of the cell.

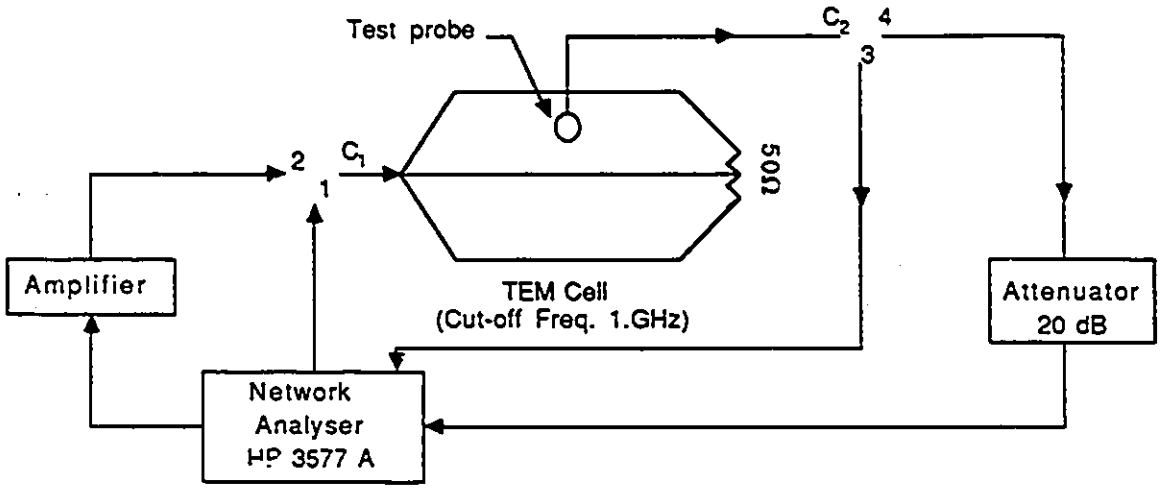

Figure 5.4: Block diagram of the transmission experiment

Before the transfer function of the sensor is measured, it is necessary to normalize the system (this removes, the electric length of the cables used, and imperfections in the source flatness).

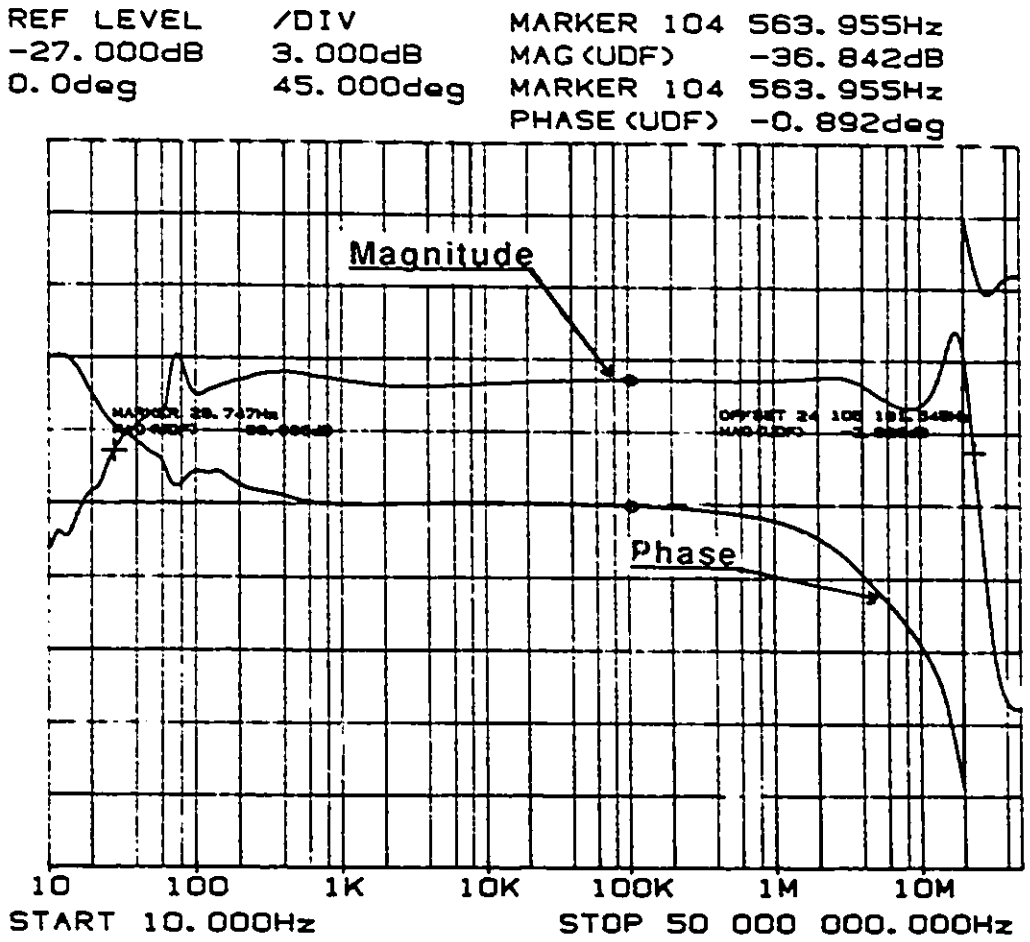

Figure 5.5: Transfer function of the magnetic field sensor

A typical transfer function is shown in Figure 5.5. It has been obtained with an input level set to the Network Analyzer (NA) at 8 dBm corresponding to the magnetic field intensity of H_{TEM} = 5.54 mA/m (rms) in the TEM cell (the procedure followed to compute H_{TEM} is given in the next section). The magnitude

of the transfer function is within ± 3 dB for frequencies between 30 Hz and 25 MHz. The phase deviates from constant by ±45° for frequencies from 30 Hz to 5 MHz (the difference in bandwidth between the magnitude and phase is due to the tune-out capacitance used to compensate in part the equivalent stray capacitance of the antenna and the transformer). In the next sections, the probe performance is evaluated in more details by measuring its sensitivity, dynamic range and noise level.

Sensitivity

The sensitivity is defined as the ratio of the output voltage to the strength of the magnetic field perpendicular to the coil plane (i.e parallel to the ferrite rod); it is equal to:

$$S_e = \frac{V_{out}}{H_{TEM}} \tag{5.2}$$

The magnetic field H_{TEM} can be expressed as:

$$H_{TEM} = \frac{V_{TEM}}{\eta\, d} \tag{5.3}$$

where

V_{TEM} rms voltage between the septum and the outer surface of the TEM cell.

η intrinsic impedance for the free space ($\eta = E_{TEM}/H_{TEM} = 377\ \Omega$).

E_{TEM} electric field in the TEM cell.

d distance between the septum to the outer surface of the TEM cell (d=8.5 cm for the TEM cell used).

Combining equations (5.2) and (5.3), the sensitivity can be calculated from the magnitude of the transfer function (T) as:

$$S_r = \frac{V_{out}}{V_{TEM}} \eta \, d \tag{5.4}$$

V_{TEM} equals 22.4 mV for a power entering the TEM cell P_{TEM}=-20 dBm. For such conditions, the output voltage is found equal to V_{out} = 0.33 mV. The sensitivity is then found equal to $S_r = 0.475 V/A\,m^{-1}$.

Electric Field Response

The septum of the TEM cell is a horizontal plane. The E-field inside is therefore vertical whereas the H-field is horizontal. The loop is positioned perpendicular to that in Figure 5.4. Figure 5.6 indicates the electric field response of the probe when it is positioned as indicated above. It shows that the electric field interference due to the 60 Hz power lines and its harmonics is important. The same results were obtained when this experiment was performed in a shielded room (the power supply of the electronic circuit can't be taken outside the shielded room). This result proves that the 60 Hz noise is not picked up by the loop antenna but by the leads of the electronic circuit. From mid-band frequencies, the response of the probe to the electric field is 40 dB below that of the magnetic field; this result

can theoretically be justified by the balanced configuration of the probe which is well suited for the great reduction of the common mode electric field noise pick-up. However, as was shown before, the configuration of the probe cannot be made perfectly balanced. This results in the deterioration of the common mode rejection ratio of the circuit which in turn favors the electric field noise pick-up.

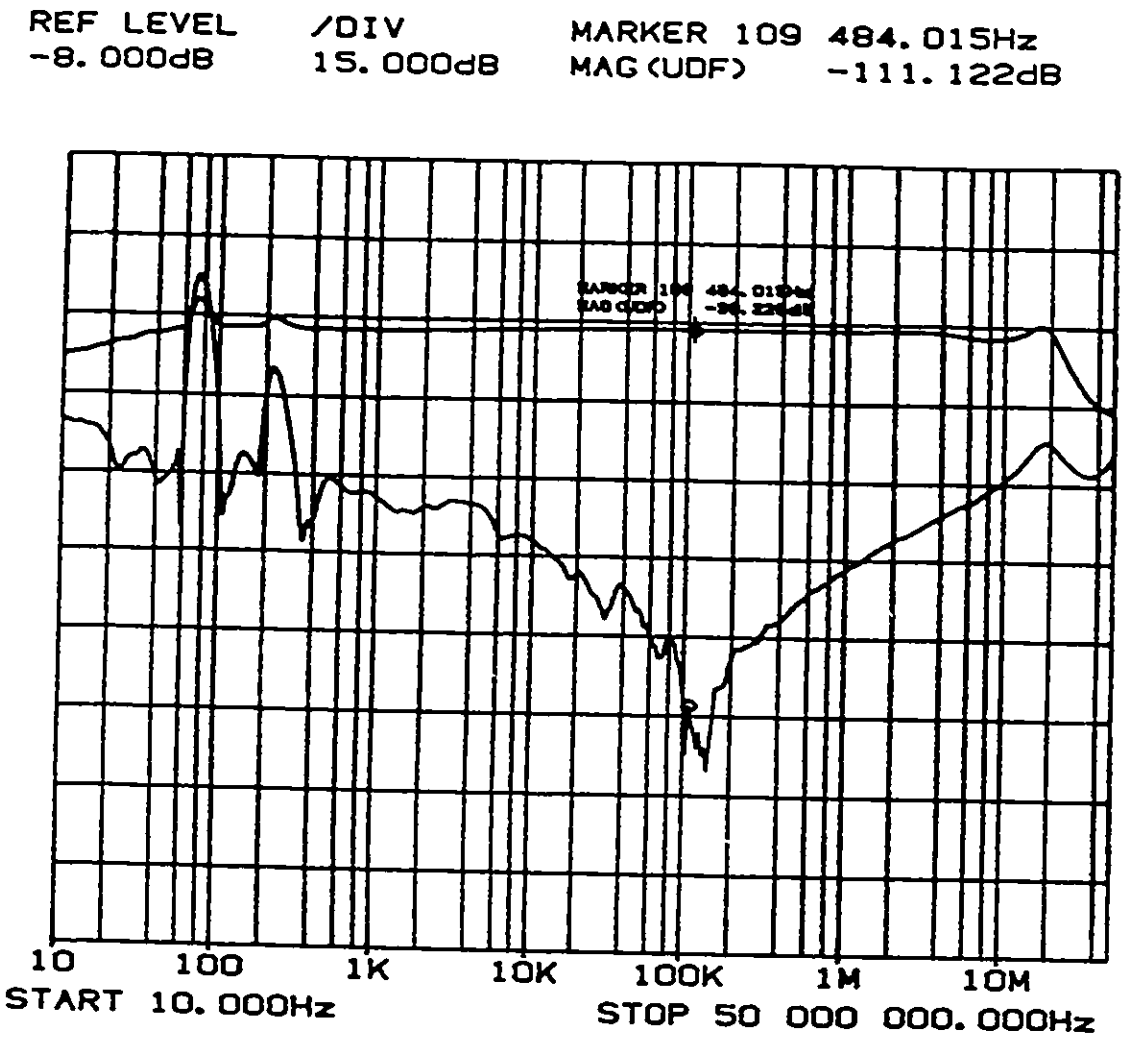

Figure 5.6: Electric field interference

Dynamic Range

The dynamic range of the sensor was measured as in Figure 5.4 (nodes "C_1.2" and "C_2.4" are connected). The 25 W amplifier was used to strengthen the magnetic field inside the TEM cell. Its gain was set to 42 dB. For various values of P_{TEM}, starting from -13 dBm up to 27 dBm, the transfer function is plotted as shown in Figure 5.7.

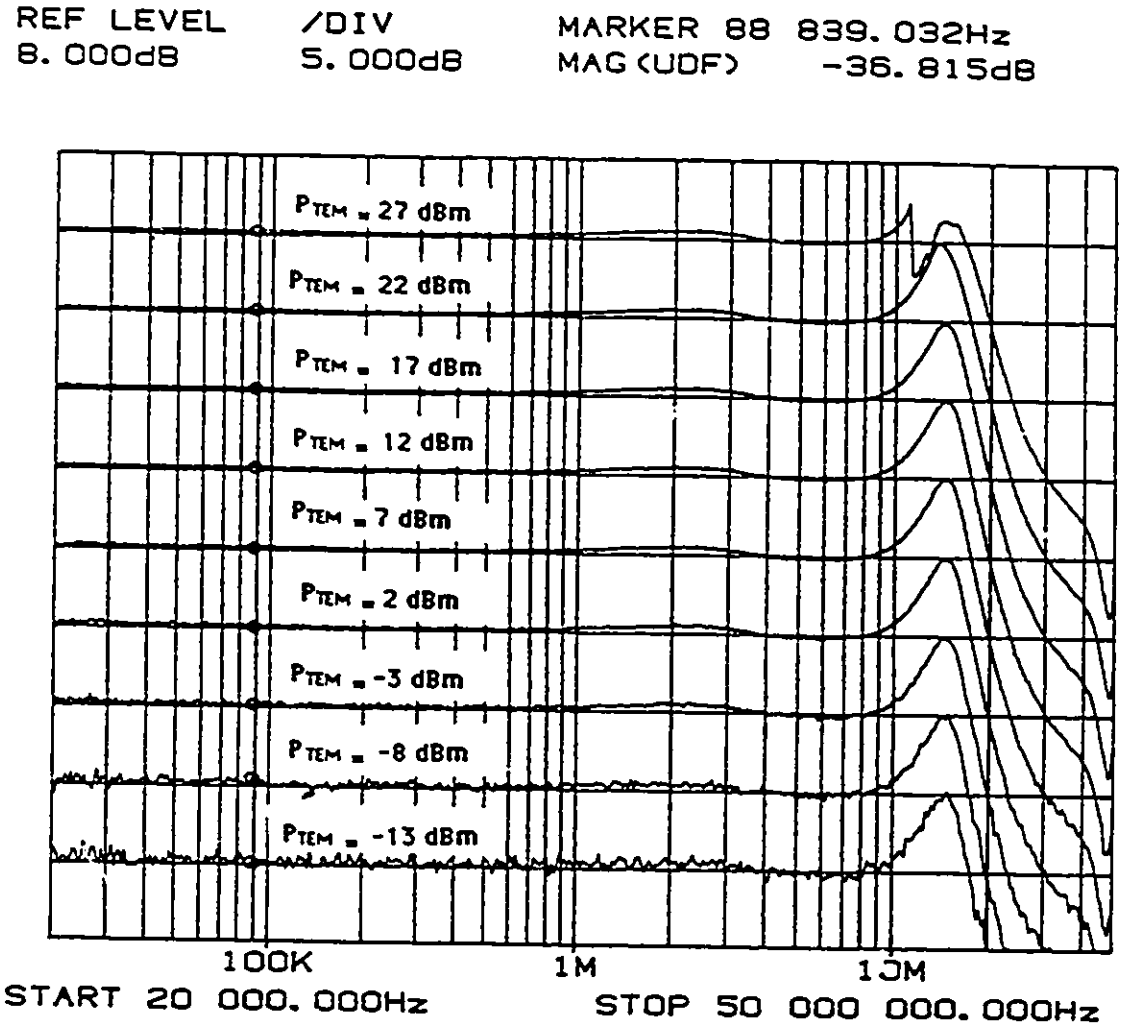

Figure 5.7: Dynamic range measurement of the sensor

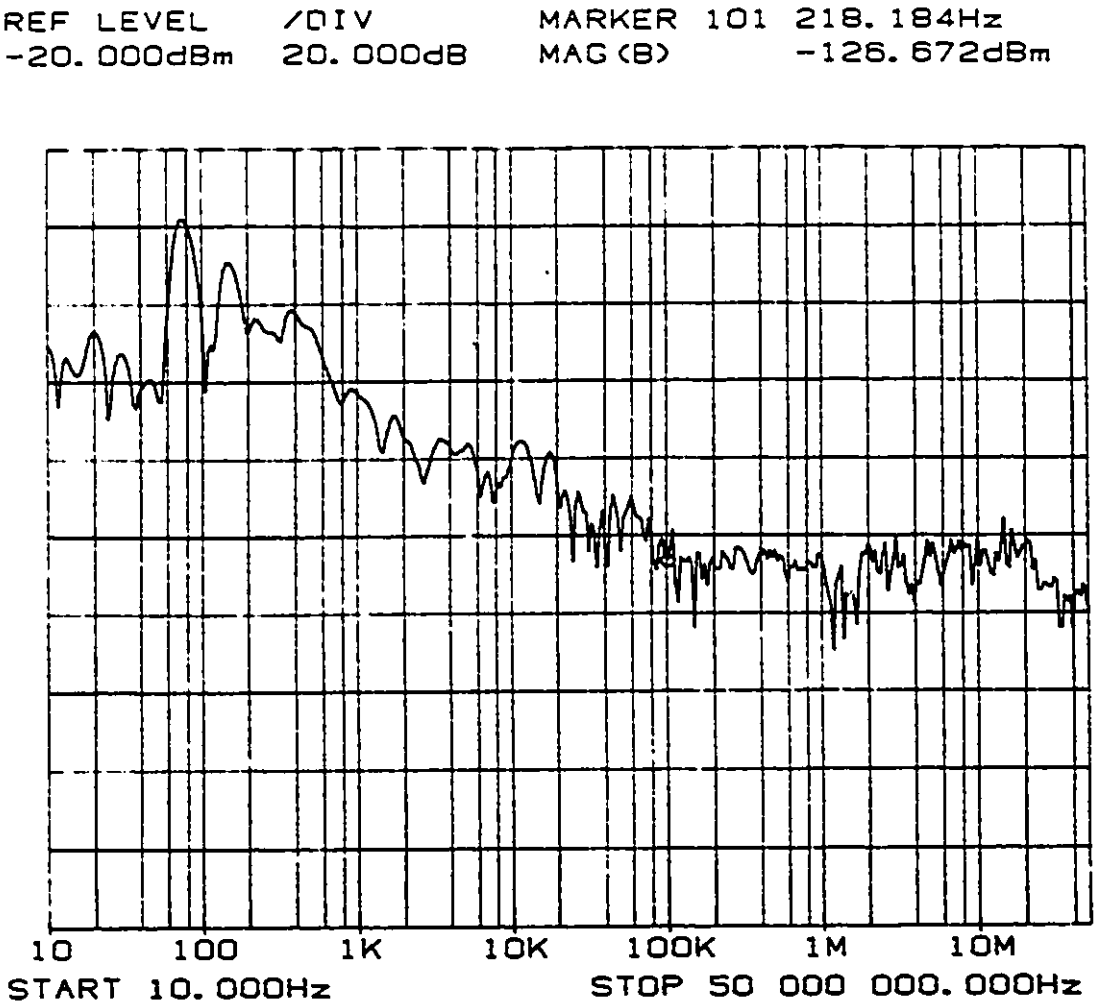

Figure 5.8: Noise level of the sensor

The noise level was measured. as indicated in Figure 5.8. It is very small at mid-band frequencies (-126 dBm at around 100 kHz). It can be seen from Figure 5.7 that a high frequency distortion starts to appear at a power entering the TEM cell of P_{TEM} equals 27 dBm. The dynamic range of the sensor is hence greater than 40 dB.

5.2.2 Time Domain

The input pulses were produced by an HP 8082A pulse generator with various rise and fall times. The pulses were then recorded using the 11802 digitizing sampling oscilloscope. Figure 5.9 shows the response of the probe to an input pulse of a width of approximately 620 ns. Two pulses are shown; one is the pulse at the input of the TEM cell and the other is at the output of the sensor.

From this Figure, it is seen that the magnetic probe output is nearly identical to the input pulse for the pulse width selected. The percent droop of the output pulses is fairly small and their rise and fall times follow those of the input pulses up to certain limit. The percent droop δ and the rise time limit t_r of the output pulse can be expressed by [42]:

$$\delta = \frac{f_1 \, t_d}{0.0035} \tag{5.5}$$

and,

$$t_r \approx \frac{0.35}{f_2} \tag{5.6}$$

where

f_1 : Low 3db roll-off frequency of the probe.
f_2 : High 3db roll-off frequency of the probe.
t_d : Input pulse width.

The low 3 dB roll-off frequency is found equal to 30 Hz. This will yield to a percent droop of $\delta = 3.6\%$ for the 620 ns pulse width selected.

Table 5.3 indicates the measurement of the rise and fall time of the output pulse for different rise and fall times of the input pulse. The rise and fall times of

the output pulse is measured using the 11800 series digital sampling oscilloscope [48]. Values were obtained by averaging several samples of measurements to avoid errors introduced by the 60 Hz power lines. This justifies the difference between the input and output rise and fall times. Table 5.3 shows also that there is a limiting rise time in the output waveform which is associated with the upper frequency roll-off of the sensor (equation (5.6)). In our experiment, the rise time limit was found approximately equal to 13 ns. This gives, using equation 5.6, a high roll-off frequency of $f_2 = 27$ MHz which is the same as that found from the frequency domain measurements within the errors of calculation. For a faster rise time, consistent overshoots which are due to the effects of the stray capacitances in the circuit are obtained.

Table 5.3: Rise and Fall Time Measurements

Input pulse		*Output Pulse*	
Rise Time (ns)	Fall Time (ns)	Rise Time (ns)	Fall Times (ns)
108.6	108.9	98	94.8
31.9	31.9	29.3	30.58
12.6	12.8	12.8	11.7
3	3	12.9	11.9

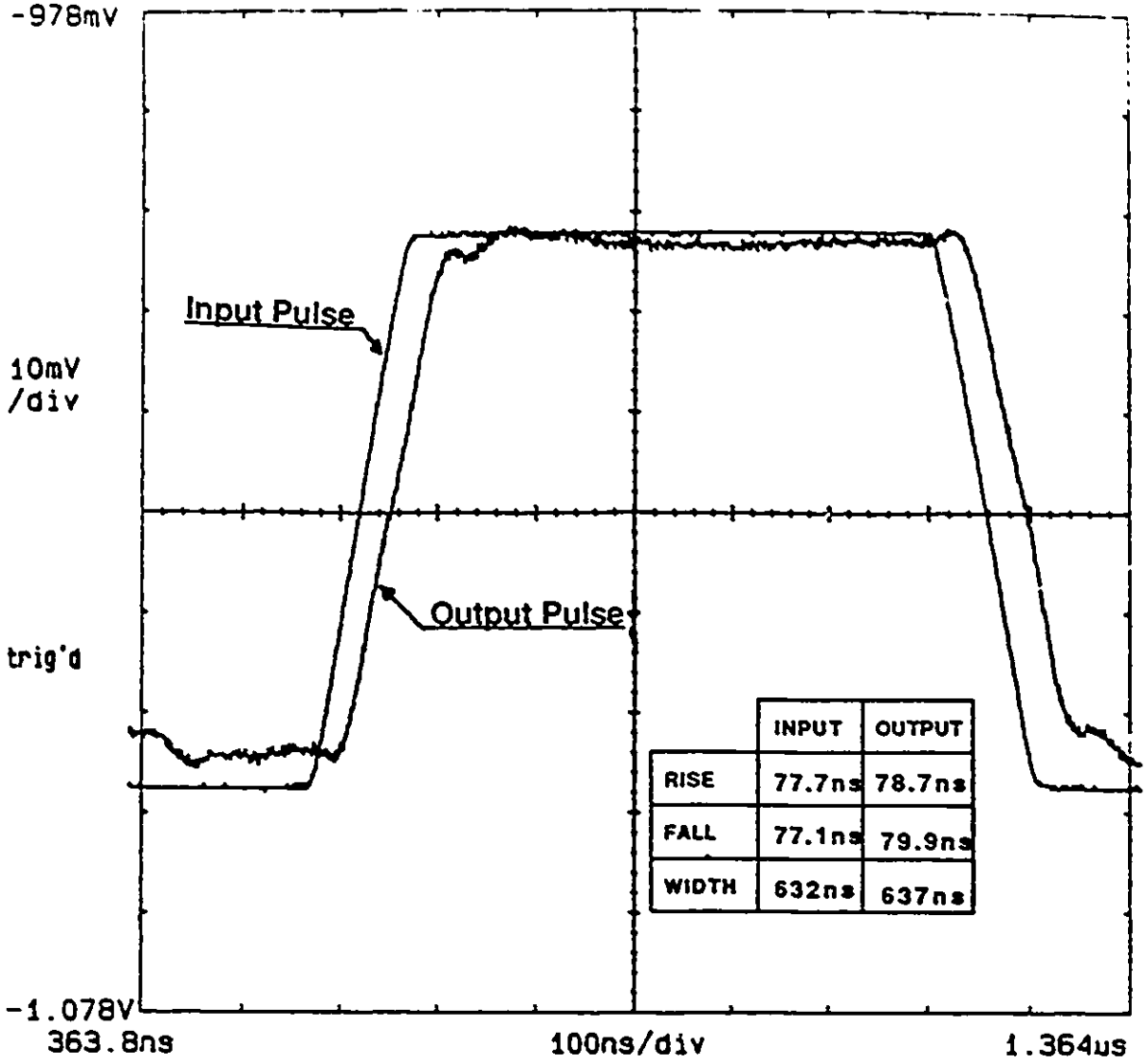

Figure 5.9: Pulse response of the sensor

Chapter 6

Conclusions and Recommendations

In this thesis, the feasibility of designing broad-band magnetic field sensors using ferrite core loop antenna has been investigated. The sensor studied consists of an electrically small loop antenna, ferrite core and a trans-impedance amplifier. Constant amplitude and phase were the main requirements for the sensor to be suitable for measurements of transient or pulsed fields including the power line frequency (60 Hz).

1. The initial stage of the work was to evaluate the low frequency limit of the sensor with an air loop antenna. An example of low frequency analysis was carried out on a magnetic field sensor recently developed at the University of Ottawa [27]. Three equations for low frequency design of the sensor were derived. Simulation was carried out to show that the sensor loop roll-off frequency is usually higher than the other roll-off frequencies due to the transformers, and therefore is a critical parameter in the design.

2. The second stage was to design a new broadband magnetic field sensor satisfying the requirements outlined. This sensor was modeled and simulated, in both time and frequency domains, using Hspice. Results showed that:

   - Constant gain (± 3 dB) is provided from 27 Hz to 27 MHz.
   - Constant phase (±45°) is provided from 27 Hz to 8 MHz.
   - There is very good reproduction of the input pulse to the output (for an input pulse rise time greater than 30 ns).

   Measurement followed the Hspice simulation of the sensor to find some other characteristics of the magnetic sensor and to confirm the results of the simulation. Experimental results show that:

   - Constant amplitude (± 3 dB) of the sensor output is provided for a wide frequency range going from 30 Hz to 25 MHz.
   - The phase of the output voltage of the sensor is within ±45° constant from 30 Hz up to 5 MHz. The difference between the high roll-off frequencies of the amplitude and phase of the output is due to the capacitance that is inserted in the front stage of the electronic circuit to compensate, in part, the winding capacitance of the loop antenna and the transformer.
   - The sensor provides a sensitivity of $S_e = 0.48V/Am^{-1}$.
   - The electric field response of the sensor is 40 dB below that of the magnetic field and this at around 100 kHz. At low frequencies, the sensor electric field response to the 60 Hz power line frequency and its har-

monics is important. This is believed due to the leads and connections from the power supply to the electronic circuit.

- The dynamic range of the sensor is greater than 40 dB.
- Transient analysis of the sensor output shows that a good pulse reproduction can be obtained for an input pulse rise time greater than 30 ns.

A good agreement has been obtained between simulated and measured results. The differences that exist between the experimental and simulated high roll-off frequency are small and within the uncertainties of measurements and values of the parameters used in the simulation. The main differences are due to the fact that the transformer leakage inductances have been neglected during our simulation.

The sensor high roll-off frequency is limited by the resonant frequency of the ferrite rod antenna. It can be increased by changing the length of the rod but this will increase losses and yield relatively big antennas. Besides that, when the length of the rod is increased, the low roll-off frequency of the ferrite rod antenna will be further decreased. The high roll-off frequency of the sensor will decrease such that the length of the rod will worsen the high frequency performance of the probe.

The designed probe can be used when measurements of low frequency magnetic fields are required. The self resonant frequency of the ferrite rod material limits the high frequency performance of the probe. Future improvement in the ferrite material properties will certainly extend the use of this design to higher

frequencies magnetic field measurements.

Future improvement of this design should take into consideration the following suggestions:

- Optimize further the design of the ferrite loop antenna. A special study should be made to optimize the rod length and ferrite material.
- Improve the electric field response of the 60 Hz and its harmonics by using a completely shielded box for the electronic circuit and providing batteries for the electronic circuit power supply.

Appendix A

Inductance of a Single Layer Solenoid

The self inductance of a long, thin solenoidal coil consisting of a single layer, wound so that the insulating gap between successive turns is negligeable is given by [51]:

$$L_a = \frac{\mu N^2 A}{l_c} \tag{A.1}$$

where, N is the number of turns, l_c is the length of the coil and A is the cross sectional area of the turns ($A = \pi b^2$ for turns of radius b).

For coils of a limited length, the field is no longer uniform and the inductance is a function of the ratio length to its to radius. The value of L_a should be multiplied by a correction factor K known as Nagaoka's constant, and which could be evaluated by mean of the following formula [51]:

$$K = \frac{1}{1 + 0.9(\frac{b}{l_c}) - 0.02(\frac{b}{l_c})^2} \tag{A.2}$$

If the turns are spaced apart, a correction factor should be taken into account so that the inductance has to be multiplied by:

$$C_{orr} = 1 - \frac{l_c\,(A+B)}{\pi\, b\, N\, K} \tag{A.3}$$

where

$$A = 2.3 \log \frac{3.46\, b}{\bar{s}} \tag{A.4}$$

and

$$B = 0.036(1 - \frac{2.5}{N} + 3.8N^2). \tag{A.5}$$

$\bar{s}$ is the center-to-center distance between two successive turns.

Appendix B

Theory of a Wideband Transformer

The transformer shown in Figure (B.1) consists of two copper coils physically placed so that the magnetic field in one links the magnetic field of the other, through a ferromagnetic (ferrite) core.

When one coil, primary, is connected to a generator, the other coil, secondary, is connected to a load, an alternating current in the primary coil will produce an alternating magnetic field common to both coils. This results in the transfer of electric energy from the input circuit to the output coil and the load [34].

The voltages induced in the primary and secondary are proportional to the number of turns (N_1, N_2) in the respective coil:

$$\frac{V_1}{V_2} = \frac{N_1}{N_2} = N_t \tag{B.1}$$

N_t is called the turn ratio of the transformer.

If there is a perfect magnetic coupling and no loss of energy in form of heat,

the output power equals to the input power which yields to the following current relationship between primary and secondary:

$$\frac{I_2}{I_1} = \frac{N_1}{N_2} = N_t \tag{B.2}$$

To obtain a relationship in terms of impedance, we multiply equations (B.1) by (B.2):

$$\frac{Z_1}{Z_2} = N_t^2 \tag{B.3}$$

Its for that reason that transformer can be used for impedance transformation purposes.

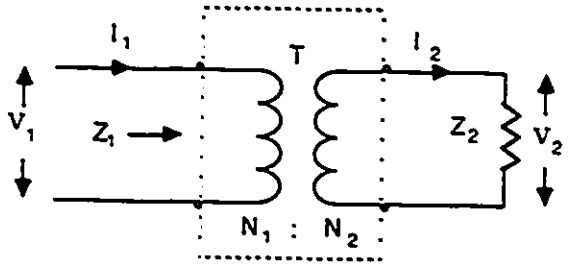

Figure B.1: Transformer Diagram

Broad-band transformers use magnetic cores and are designed to transfer energy over a wideband of frequency. Their equivalent circuit is as shown in Figure B.2 [15].

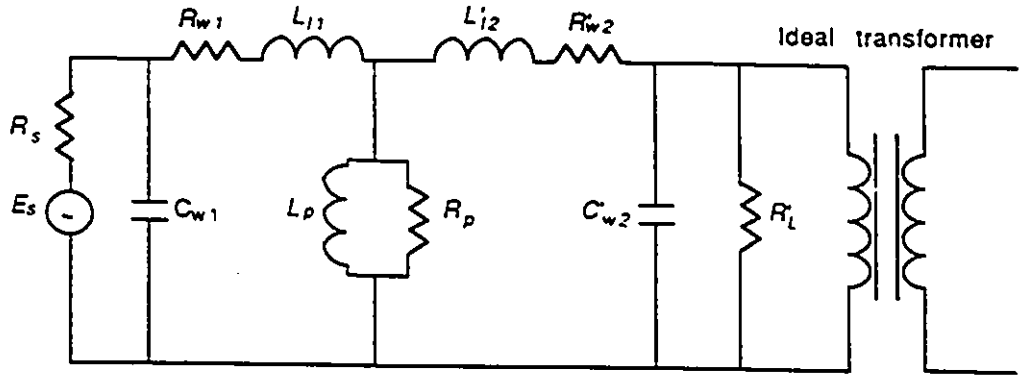

Figure B.2: Lumped equivalent circuit of the transformer

where

E_s source voltage.

R_s source resistance.

C_{w1} primary winding capacitance.

C'_{w2} secondary capacitance referred to primary side.

R_{w1} resitance of primary winding.

R'_{w2} secondary resistance referred to primary side.

L_{l1} primary leakage inductance.

L'_{l2} secondary leakage inductance referred to the primary side.

L_p inductance due to magnetic core.

R_p Losses due to magnetic core.

R_L' Load resistance referred to primary side.

The 3 dB roll-off frequency is given by:

$$f_{3dB} = \frac{R}{L_p} \tag{B.4}$$

where R is the sum of the winding and source resistance. At high frequencies, the linkage of magnetic flux between primary and secondary windings is in general not complete. The difference, or the leakage flux associated with the leakage inductance, limits the high frequency transfer function of the transformer [40]. The interwinding and stray capacitances are also important in determining the high frequency performance of the transformer. When single layer windings and toroid cores of appropriate sizes are utilized, the capacitance between the windings can be made small.

Appendix C

Optimization of the Low Cut-off frequency of the Previous Sensor

The nonlinear multivariable optimization Subroutine, NCONF (taken from the International Mathematics and Scientific Library), was used to minimize f_{sens}.

Designation of functions and parameters is as follows:

CALL(FCN,M,ME,N,XGUESS,IBTYPE,XLB,XUB,XSCALE,IPRINT,MAXITN,X,FVALUE)

Where

FCN	a user-supplied subroutine to evaluate the function at a given point.
M	total number of constraints.
ME	number of equality constraints.
N	number of variables.
X	the point at which the functions are evaluated.
XGUESS	vector of length N containing an initial guess of the of the computed solution.
IBTYPE	indicates the types of bounds on variables.

XLB	vector of length N containing the lower bounds on variables.
XUB	vector of length N containing the upper bounds on variables.
XSCALE	vector of length N containing the value of the objective function.
IPRINT	indicates the desired output level.
MAXITN	maximum number of iteration allowed.
FVALUE	scalar containing the value of the objective function.

In this Appendix, we show how the design constraints and boundary values are derived according to the different design assumptions made.

C.1 Design Assumptions

Some of the simulated results, found in Chapter 3, are taken into consideration to characterize the components of the vector X to be optimized. All the design assumptions are stated below:

- The loop wire antenna should be easy to wind and should present a small resistance per unit length. Although AWG 9 has a small resitance per unit length, it is considered to be at the limit to be easily wound. A selection of a loop wire greater than AWG 14 will give a relatively big loop resistance per unit length.

- The loop antenna should be made small and with a high sensitivity over the operating frequency range. A loop raduis "b" between 2 and 4 centimeters garantees these two design conditions for a loop antenna number of turns $N_a = 10$ turns.

- The secondary coil of the two transformers should be easy to wind around the toroid selected and should give a small resistance per unit length. Secondary coils of a gauge between AWG 23 and AWG 32 is suitable with the geometry of the toroids selected.

- The same number of secondary turns (N_{t1}, N_{t2}) of the secondary winding of both transformers, equal to 15 is assumed (see analysis in 3.3).

- R_{amp} equals 0.7 Ω.

All the assumptions made are summarized in Table C.1.

Table C.1: Assumed design values

N_a	10
N_{t1}	15
N_{t2}	15
l_w (mm)	19
b (cm)	$2 \leq b \leq 4$
(AWG) of the loop	$9 \leq AWG \leq 16$
(AWG) of the transformer	$23 \leq AWG \leq 32$

C.2 Design Equations

The minimization of f_{sens} is related to the optimal choice of the loop wire as well as that of the transformer since all the components of the vector X depend on them. It is therefore necessary to express f_{sens} as a factor of $(x_i), i = 1, ..., 5$. Where

x_1 resistance per one secondary turn.

x_2 total length of the loop antenna wire.

x_3 resistance per unit length of the wire of the loop.

x_4 the radius of the loop (b).

x_5 the radius of the wire of the loop (a).

The resistance R of a copper wire of, length l, resistivity ρ, and diameter d, at low frequencies can be expressed as:

$$R = \rho \frac{4l}{\pi d^2} \tag{C.1}$$

For the loop antenna, the resistance is:

$$R_a = l_a R_{wa} \tag{C.2}$$

where

l_a : is the length of the loop conductor.
R_{wa} : is the resistance of the loop conductor per unit length.

R_{wa} and l_a can be expressed by:

$$R_{wa} = \frac{\rho}{\pi a^2} \tag{C.3}$$

$$l_a = b\, N_a + C \tag{C.4}$$

where " C " is a correction factor due to the spacing between the loops and the wire in the end connections. The parameter "C" is measured and found equal to 7 cm for $N_a = 10$.

The resistance of the loop antenna can be expressed as a function of X as follows:

$$R_a = \frac{(2\,N_a\,\pi\,x_3 + C)\,\rho}{x_3^2} \qquad (C.5)$$

The low frequency winding resistance of a transformer is expressed by:

$$R_w = N_t R_{wt}(d_2 - d_1 + 2h) \qquad (C.6)$$

where

N_t secondary number of turns of the transformer.

R_{wt} the resistance per unit length of the wire of the transformer.

d_2 outer diameter of the toroid.

d_1 inner diameter of the toroid.

h height of the toroid.

Where:

$$R_{wt} = \frac{4\rho}{\pi d^2_{wt}} \qquad (C.7)$$

where d_{wt} is the diameter of the transformer wire.

The winding resistance is therefore:

$$R_w = 4N_t(d_2 - d_1 + 2h)\frac{\rho}{\pi d^2_{wt}} \qquad (C.8)$$

C.3 Parameter Inter-relationships

Two components in the X vector are interrelated.

- The radius of the loop (x_4) is related to the total length of the loop antenna (x_2) by:

$$x_2 = 2\pi N_a x_4 + C \tag{C.9}$$

- The resistance per unit length of the wire of the loop x_3 is related to the radius of the wire of the loop x_4 by:

$$x_3 = \frac{\rho}{\pi x_5^2} \tag{C.10}$$

In this case of minimization, there are no inequality constraints.

The numerical relationships given by equations (C.9) and (C.10) are given in Table C.2.

Table C.2: Design constraints

1^{st} constraint	$x_2 = 62.4x_4 + 0.07$
2^{nd} constraint	$3.14x_3{x_5}^2 = 1.724\ 10^{-8}$

C.4 Boundary Conditions

The boundary conditions are defined here as the upper and lower bounds of the components of X vector. They can be defined by two five dimensional

vectors (X_{lb}, X_{ub}). All the bound values should satisfy equations (C.9) and (C.10). They are set according to the design assumptions that were stated at the previous sections. All those assumptions are going to be restated in this section.

The first assumption states that the coil of the transformer is made of wire with gauges between AWG 23 and AWG 32. This gives the first components of the boundary vectors:

$$X_{lb}(1) = R_{23c} l_w \tag{C.11}$$

$$X_{up}(1) = R_{32c} l_w \tag{C.12}$$

where

l_w length of one toroidal turn.

R_{23c} the resistance per unit length of the wire of gauge 23.

R_{32c} the resistance per unit length of the wire of gauge 32.

The values of R_{23c}, R_{32c}, R_{13c} and R_{9c} are obtained from Table C.4[1].

The second assumption characterizes the wire of the loop antenna that should be of gauge between AWG 9 and AWG 13. This gives the third and fifth components of the boundary vector since they are interrelated by the second constraint:

$$X_{ub}(3) = R_{13c} \tag{C.13}$$

$$X_{lb}(3) = R_{9c} \tag{C.14}$$

where

[1]This table is reproduced from Fair-Rite 10th edition [15]

R_{9c} the resistance per unit length of the wire of gauge 9.

R_{13c} the resistance per unit length of the wire of gauge 13.

The values of R_{23c} and R_{32c} are obtained from Table C.4. The fifth components of the boundary vectors were deduced from equation (C.10):

$$X_{ub}(5) = \sqrt{\frac{\rho}{\pi R_{9c}}} \tag{C.15}$$

$$X_{lb}(5) = \sqrt{\frac{\rho}{\pi R_{13c}}} \tag{C.16}$$

The third assumption states that the loop radius (x_4) should be between 2 and 4 cm. This gives the second and fourth upper and lower boundary values which are also interrelated by equation (C.9):

$$X_{ub}(2) = 2\pi N_a X_{ub}(4) + 0.07 \tag{C.17}$$

$$X_{lb}(2) = 2\pi N_a X_{lb}(4) + 0.07 \tag{C.18}$$

Table C.3 shows the numerical values of the boundary parameters.

Table C.3: Boundary values

Lower bounds		*Upper bounds*	
$X_{lb}(1)$ (Ω/turn)	798 10^{-6}	$X_{ub}(1)$ (Ω/turn)	10.2 10^{-3}
$X_{lb}(2)$ (m)	1.3	$X_{ub}(2)$ (m)	2.6
$X_{lb}(3)$ (Ω/m)	2.6 10^{-3}	$X_{ub}(3)$ (Ω/m)	13.2 10^{-3}
$X_{lb}(4)$ (m)	2 10^{-2}	$X_{ub}(4)$ (m)	4 10^{-2}
$X_{lb}(5)$ (m)	6.45 10^{-6}	$X_{ub}(5)$ (m)	1.45 10^{-2}

Table C.4: DC Resistance of Annealed Bare Copper Wire

Gauge (AWG) or (B&S)	DIAMETER INCHES			AREA	WEIGHT	LENGTH	RESISTANCE AT 68°F (20° C)		
	Min.	Nom.	Max.	Circular Mils	Pounds per M'	Feet per Lb.	Ohms per M'	Feet per Ohm	Ohms per Lb.
9	.1133	.1144	.1155	13090.	39.63	25.23	.7921	1262.	.01999
10	.1009	.1019	.1029	10380.	31.43	31.82	.9989	1001.	.03178
11	.08983	.09074	.09165	8234.	24.92	40.12	1.260	794.	.05053
12	.08000	.08081	.08162	6530.	19.77	50.59	1.588	629.6	.08035
13	.07124	.07196	.07268	5178.	15.68	63.80	2.003	499.3	.1278
14	.06344	.06408	.06472	4107.	12.43	80.44	2.525	396.0	.2032
15	.05650	.05707	.05764	3257.	9.858	101.4	3.184	314.0	.3230
16	.05031	.05082	.05133	2583.	7.818	127.9	4.016	249.0	.5136
17	.04481	.04526	.04571	2048.	6.200	161.3	5.064	197.5	.8167
18	.03990	.04030	.04070	1624.	4.917	203.4	6.385	156.5	1.299
19	.03553	.03589	.03625	1288.	3.899	256.5	8.051	124.2	2.065
20	.03164	.03196	.03228	1022.	3.092	323.4	10.15	98.5	3.283
21	.02818	.02846	.02874	810.1	2.452	407.8	12.80	78.11	5.221
22	.02510	.02535	.02560	642.4	1.945	514.2	16.14	61.95	8.301
23	.02234	.02257	.02280	509.5	1.542	648.4	20.36	49.13	13.20
24	.01990	.02010	.02030	404.0	1.223	817.7	25.67	38.96	20.99
25	.01770	.01790	.01810	320.4	.9699	1031.	32.37	30.90	33.37
26	.01578	.01594	.01610	254.1	.7692	1300.	40.81	24.50	53.06
27	.01406	.01420	.01434	201.5	.6100	1639.	51.47	19.43	84.37
28	.01251	.01264	.01277	159.8	.4837	2067.	64.90	15.41	134.2
29	.01115	.01126	.01137	126.7	.3836	2607.	81.83	12.22	213.3
30	.00993	.01003	.01013	100.5	.3042	3287.	103.2	9.691	339.2
31	.008828	.008928	.009028	79.7	.2413	4145.	130.1	7.685	539.3
32	.007850	.007950	.008050	63.21	.1913	5227.	164.1	6.095	857.6
33	.006980	.007080	.007180	50.13	.1517	6591.	206.9	4.833	1364.
34	.006205	.006305	.006405	39.75	.1203	8310.	260.9	3.833	2168.
35	.005515	.005615	.005715	31.52	.09542	10480.	329.0	3.040	3448.
36	.004900	.005000	.005100	25.00	.07568	13210.	414.8	2.411	5482.
37	.004353	.004453	.004553	19.83	.06001	16660.	523.1	1.912	8717.
38	.003865	.003965	.004065	15.72	.04759	21010.	659.6	1.516	13860.
39	.003431	.003531	.003631	12.47	.03774	26500.	831.8	1.202	22040.
40	.003045	.003145	.003245	9.888	.02993	33410.	1049.	0.9534	35040.
41	.00270	.00280	.00290	7.8400	.02373	42140.	1323.	.7559	55750.
42	.00239	.00249	.00259	6.2001	.01877	53270.	1673.	.5977	89120.
43	.00212	.00222	.00232	4.9284	.01492	67020.	2104.	.4753	141000.
44	.00187	.00197	.00207	3.8809	.01175	85100.	2672.	.3743	227380.
45	.00166	.00176	.00186	3.0976	.00938	106600.	3348.	.2987	356890.
46	.00147	.00157	.00167	2.4649	.00746	134040.	4207.	.2377	563900.

Appendix D

Equivalent Circuit Parameter Identification of the Antenna and Transformer

The equivalent circuit parameters of the antenna and transformer may be identified by measuring their impedance over a wide range of frequency. Figures D.1 and D.2 show the plots of the impedances as a function of frequency. From the magnitude response, it can be seen that above a low 3 dB cutoff frequency, f_{3dB}, the impedance increases to a value Z_p at a rate of 6 dB per octave and then decreases at a rate of -6 dB per octave, with one pole roll-off.

The following values of the phase are identified: 45° at f_{3dB}, 90° at midband frequencies, 45° when $f = f_1$, 0° when $f = f_r$, -45° when $f = f_2$ and approaches -90° as frequency increases.

The impedance of the device under test (DUT) can then be approximated by

[32]

$$Z_{DUT} = \frac{1 + \tau_f s}{s^2 + BW s + f_r^2} \tag{D.1}$$

where:

$$BW = f_2 - f_1 = \frac{f_r}{Q} \tag{D.2}$$

and

$$f_r = f_1 f_2 \tag{D.3}$$

Q is the quality factor of the DUT and s is the frequency.

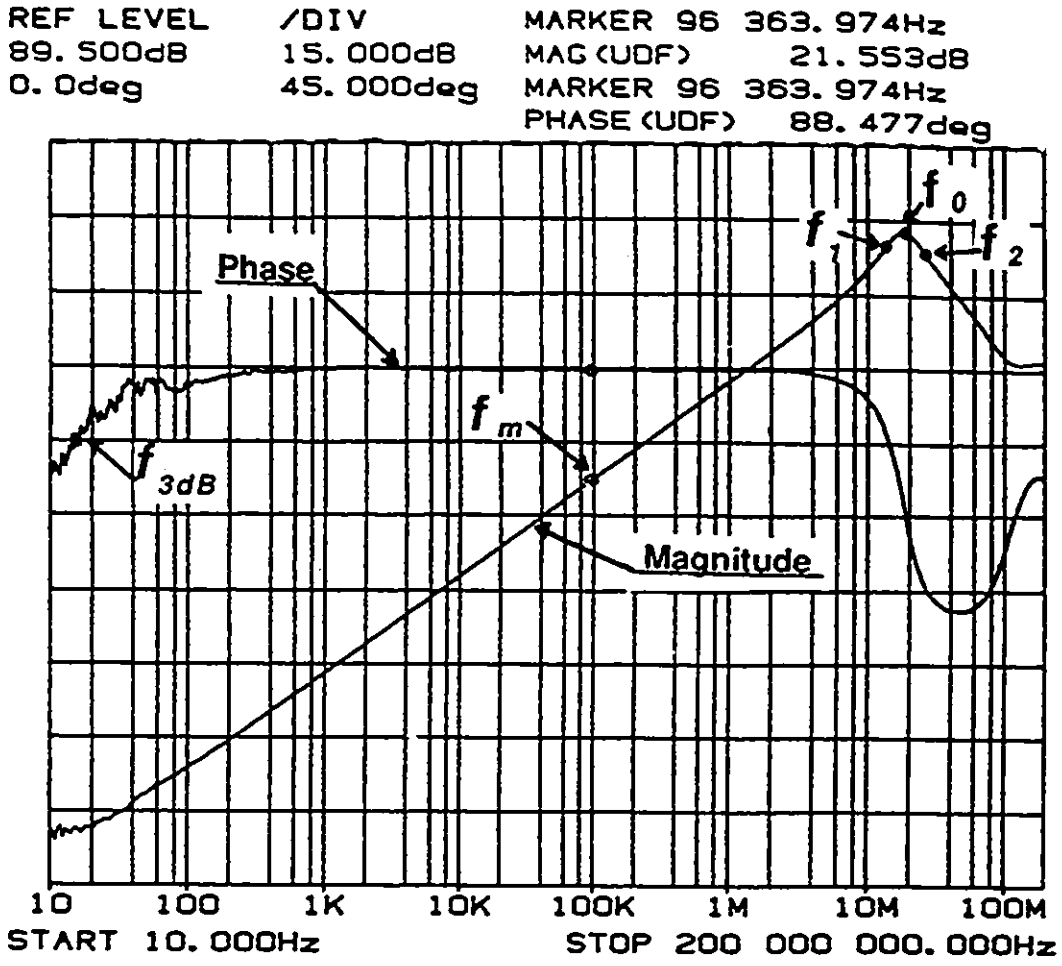

Figure D.1: Bode diagram of the loop antenna impedance

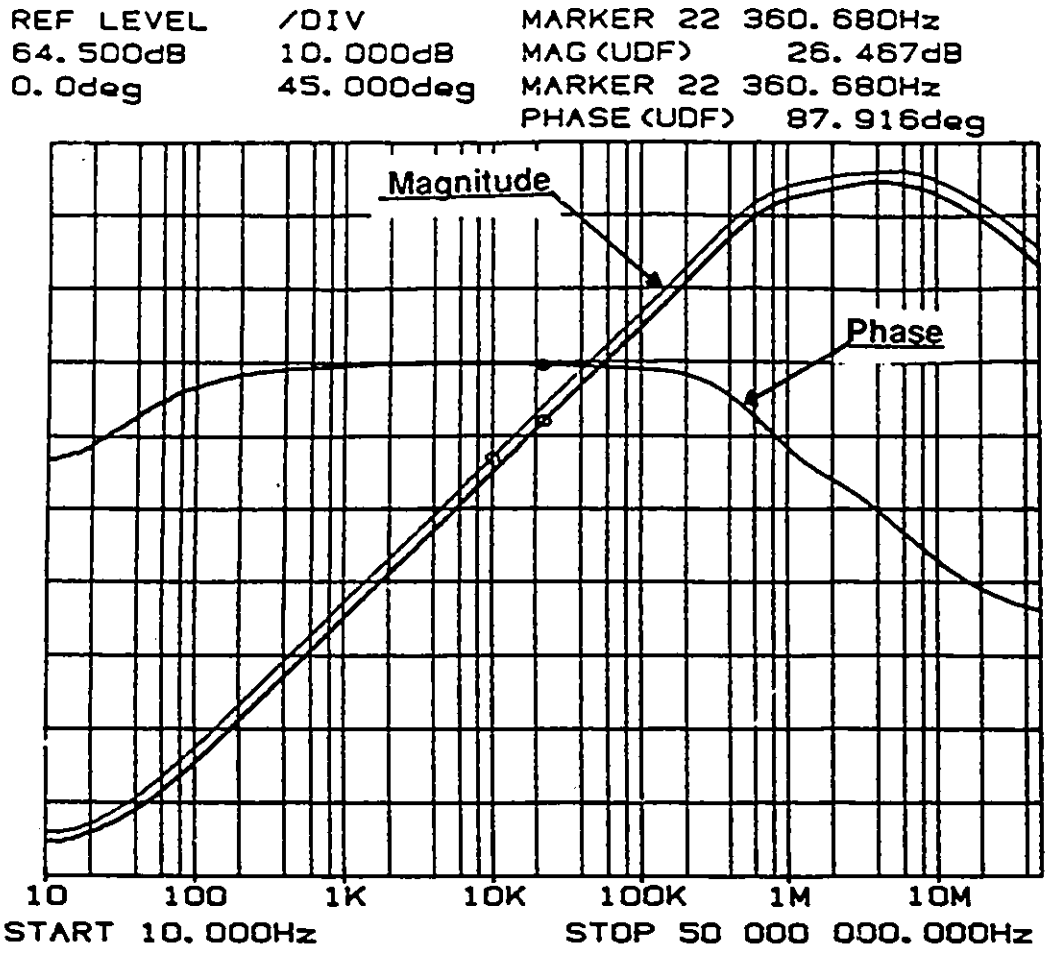

Figure D.2: Bode diagram of the secondary impedance of each side of the transformer

Figure D.3 shows the model of the DUT. where

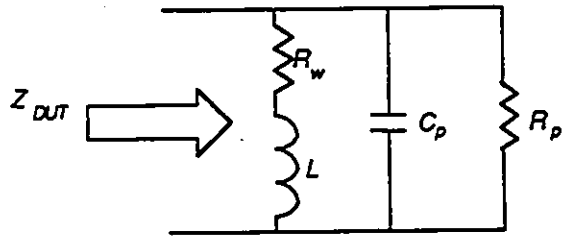

Figure D.3: Model of the DUT

R_w : winding resistance of the DUT
L : winding inductance of the DUT
R_p : core losses resistor of the DUT
C_p : stray capacitance due to winding and dielectric losses of the DUT

From the equivalent circuit, Z_{DUT} is equal to:

$$Z_{DUT} = \frac{R_w + L_s}{s^2 + (\frac{R_p}{L} + \frac{1}{R_p C_p})\, s + \frac{R_p + R_w}{R_p L C_p}} \tag{D.4}$$

Comparing the two expressions of Z_{DUT}, and neglecting the effect of R_w with respect to R_p (the winding resistance of the wire used in either the antenna or transformer has a very small resistance per unit length), it can be deduced that:

$$f_{3db} = \frac{R_w}{2\pi L} \tag{D.5}$$

$$f_r = \frac{1}{2\pi\sqrt{L\, C_p}} \tag{D.6}$$

$$BW = \frac{1}{2\pi R_p C_p} \tag{D.7}$$

The equivalent circuit parameters of the DUT could be then identified by following the procedure outlined below,

1. Specify in the Bode diagram, f_{3db}, f_1, f_2, f_r, and the amplitude of the impedance at the mid-band frequency where the phase is 90°.

2. Calculate the inductance L. L approximates to the open circuit series inductance for the transformer.

3. Calculate the winding resistance R_w from equation D.5.

4. Calculate C_p from equation D.6.

5. Deduce R_p using equation D.7.

Table D.1 summarizes the parameters calculated from this procedure.

Table D.1: Parameters of the DUT

parameters	*Loop Antenna*	*Transformer*	
		Side 1	Side 2
$L\,(\mu H)$	19.7	148.7	187.7
$R_w\,(m\Omega)$	2	23.9	26.7
$C_p\,(pF)$	3.55	10.6	7.8
$R_p\,(k\Omega)$	3.4	0.91	1.18

Appendix E

Component Values, Program Listings and Data Sheets

This Appendix gives the values of all the components used in both the old and new design of the magnetic field sensor. The operational amplifiers data sheets are also given.

E.1 Characteristics of the Magnetic Sensors

E.1.1 Old Design

The characteristics of all the components used in the previous design of the magnetic field sensor are summarized in Table E.1.

Table E.1: Old design parameter values

Operational Amplifier	OPA621
Transformer coil	AWG 24
Loop wire gauge	AWG 9
Initial permeability	4300
R_f	560Ω

E.1.2 New Design

The characteristics of all the components used in the new design of the magnetic field sensor are summarized in Table E.2.

Table E.2: New design parameter values

C_f	50pf
R_f	272Ω
R_1	164Ω
R_2	1000Ω
R_m	39.2Ω
N_{t1}	8
N_{t2}	8

Differential amplifier AD9618

Current follower OP37

Loop wire gauge AWG 9

Ferrite rod material #33

Transformer coil gauge AWG 24

E.2 Data Sheets

- **OP37 Operational Amplifier**

Model		AD OP-37G			AD OP-37F			AD OP-37E		
Parameter	**Symbol**	**Min**	**Typ**	**Max**	**Min**	**Typ**	**Max**	**Min**	**Typ**	**Max**
OPEN LOOP GAIN	A_{VO}	700	1,500		1,000	1,800		1,000	1,800	
		400	1,500		800	1,500		800	1,500	
		200	500		250	700		250	700	
		450	1,000		700	1,300		750	1,500	
OUTPUT CHARACTERISTICS										
Voltage Swing	V_O	±11.5	±13.5		±12.0	±13.8		±12.0	±13.8	
		±10.0	±11.5		±10.0	±11.5		±10.0	±11.5	
		±11.0	±13.3		±11.4	±13.5		±11.7	±13.6	
Open-Loop Output Resistance	R_O		70			70			70	
FREQUENCY RESPONSE										
Gain Bandwidth Product	GBW	45	63		45	63		45	63	
		–	40		–	40		–	40	
Slew Rate	SR	11	17		11	17		11	17	
INPUT OFFSET VOLTAGE										
Initial	V_{OS}		30	100		20	60		10	25
			55	220		40	140		20	60
Average Drift	TCV_{OS}		0.4	1.8		0.3	1.3		0.2	0.6
Long-Term Stability	V_{OS}/Time		0.4	2.0		0.3	1.5		0.2	1.0
Adjustment Range			±4.0			±4.0			±4.0	
INPUT BIAS CURRENT										
Initial	I_B		±15	±80		±12	±55		±10	±40
			±25	±150		±18	±95		±14	±60
INPUT OFFSET CURRENT										
Initial	I_{OS}		12	75		9	50		7	35
			20	135		14	85		10	50
INPUT NOISE										
Voltage	e_{n} p-p		0.09	0.25		0.08	0.18		0.08	0.18
Voltage Density	e_n		3.8	8.0		3.5	5.5		3.5	5.5
			3.3	5.6		3.1	4.5		3.1	4.5
			3.2	4.5		3.0	3.8		3.0	3.8
Current Density	i_n		1.7	–		1.7	4.0		1.7	4.0
			1.0	–		1.0	2.3		1.0	2.3
			0.4	0.6		0.4	0.6		0.4	0.6
INPUT VOLTAGE RANGE										
Common Mode	CMVR	±11.0	±12.3		±11.0	±12.3		±11.0	±12.3	
		±10.5	±11.8		±10.5	±11.8		±10.5	±11.8	
Common-Mode Rejection Ratio	CMRR	100	120		106	123		114	126	
		96	118		102	121		110	124	
INPUT RESISTANCE										
Differential	R_{IN}	0.8	4		1.2	5		1.5	6	
Common Mode	R_{INCM}		2			2.5			3	
POWER SUPPLY										
Rated Performance			±15			±15			±15	
Operating			±(4–18)			±(4–18)			±(4–18)	
Current, Quiescent	I_Q		3.3	5.6		3.0	4.6		3.0	4.6
Rejection	PSR		2	20		1	10		1	10
			2	32		2	16		2	15
Power Consumption	P_d		100	170		90	140		90	140
OPERATING TEMPERATURE RANGE	T_{min}, T_{max}	–25		+85	–25		+85	–25		+85
PACKAGE OPTIONS[3]										
Plastic Mini-DIP (N-8)			AD OP-37GN			AD OP-37FN			AD OP-37EN	
Cerdip (Q-8)			AD OP-37GQ			AD OP-37FQ			AD OP-37EQ	
TO-99 (H-08)			AD OP-37GH			AD OP-37FH			AD OP-37EH	

AD OP-37C			AD OP-37B			AD OP-37A			Conditions	Units
Min	Typ	Max	Min	Typ	Max	Min	Typ	Max		
700	1,500		1,000	1,800		1,000	1,800		R_L = 2kΩ, V_{OUT} = ± 10V	V/mV
400	1,500		800	1,500		800	1,500		R_L = 1kΩ, V_{OUT} = ± 10V	V/mV
200	500		250	700		250	700		R_L = 600Ω, V_{OUT} = ± 1V, V_S = ± 4V	V/mV
300	800		500	1,000		600	1,200		R_L = 2kΩ, V_{OUT} = ± 10V, T_A = min to max	V/mV
± 11.5	± 13.5		± 12.0	± 13.8		± 12.0	± 13.8		R_L = 2kΩ	V
± 10.0	± 11.5		± 10.0	± 11.5		± 10.0	± 11.5		R_L = 600Ω	V
± 10.5	± 13.0		± 11.0	± 13.2		± 11.5	± 13.5		R_L = 2kΩ, T_A = min to max	V
	70			70			70		I_{OUT} = 0A, V_{OUT} = 0V	Ω
45	63		45	63		45	63		f_O = 10kHz	MHz
–	63		–	40		–	40		f_O = 1MHz	MHz
11	17		11	17		11	17		R_L = 2kΩ	V/μs
	30	100		20	60		10	25	(Note 1)	μV
	70	300		50	200		30	60	T_A = min to max	μV
	0.4	1.8		0.3	1.3		0.2	0.6	T_A = min to max	μV/°C
	0.4	2.0		0.3	1.5		0.2	1.0	(Note 2)	μV/month
	± 4.0			± 4.0			± 4.0		R_S = 10kΩ	mV
	± 15	± 80		± 12	± 55		± 10	± 40		nA
	± 35	± 150		± 28	± 95		± 20	± 60	T_A = min to max	nA
	12	75		9	50		7	35		nA
	30	135		22	85		15	50	T_A = min to max	nA
	0.09	0.25		0.08	0.18		0.08	0.18	0.1Hz to 10Hz	μV p-p
	3.8	8.0		3.5	5.5		3.5	5.5	f_O = 10Hz	nV/√Hz
	3.3	5.6		3.1	4.5		3.1	4.5	f_O = 30Hz	nV/√Hz
	3.2	4.5		3.0	3.8		3.0	3.8	f_O = 1000Hz	nV/√Hz
	1.7	–		1.7	4.0		1.7	4.0	f_O = 10Hz	pA/√Hz
	1.0	–		1.0	2.3		1.0	2.3	f_O = 30Hz	pA/√Hz
	0.4	0.6		0.4	0.6		0.4	0.6	f_O = 1000Hz	pA/√Hz
± 11.0	± 12.3		± 11.0	± 12.3		± 11.0	± 12.3			V
± 10.2	± 11.5		± 10.3	± 11.5		± 10.3	± 11.5		T_A = min to max	V
100	120		106	123		114	126		V_{CM} = ± 11V	dB
94	116		100	119		108	122		V_{CM} = ± 10V, T_A = min to max	dB
0.8	4		1.2	5		1.5	6			MΩ
	2			2.5			3			GΩ
	± 15			± 15			± 15			V
	± (4–18)			± (4–18)			± (4–18)			V
	3.3	5.6		3.0	4.6		3.0	4.6	V_S = ± 15V	mA
	2	20		1	10		1	10	V_S = ± 4V to ± 18V	μV/V
	4	51		2	20		2	16	V_S = ± 4.5V to ± 18V, T_A = min to max	μV/V
	100	170		90	140		90	140	V_{OUT} = 0V	mW
–55		+125	–55		+125	–55		+125		°C
ADOP-37CQ ADOP-37CH			ADOP-37BQ ADOP-37BH			ADOP-37AQ ADOP-37AH				

Specifications shown in boldface are tested on all production units at final electrical test. Results from those tests are used to calculate outgoing quality levels. All min and max specifications are guaranteed, although only those shown in boldface are tested on all production units.

DC ELECTRICAL CHARACTERISTICS (Unless otherwise noted, A_V = +10; $\pm V_S$ = ±5 V; R_f = 1000 Ω; R_{LOAD} = 100 Ω)

Parameter	Conditions	Temp	Test Level	Mil Sub[4]	AD9618JN/JR Min	AD9618JN/JR Typ	AD9618JN/JR Max	AD9618AQ/SQ/SZ/883B[4] Min	AD9618AQ/SQ/SZ/883B[4] Typ	AD9618AQ/SQ/SZ/883B[4] Max	AD9618BQ/TQ/TZ/883B[4] Min	AD9618BQ/TQ/TZ/883B[4] Typ	AD9618BQ/TQ/TZ/883B[4] Max	Units
Input Offset Voltage[1, 4]		+25°C	I	1	−1.1	+0.5	+2.2	−1.1	−0.5	+2.2	0.0	+0.5	+1.1	mV
Input Offset Voltage TC[5]		Full	IV		−4	+3	+25	−4	+3	+25	−4	+3	+25	µV/°C
Input Bias Current[4]														
Inverting		+25°C	I	1	−45	0	+45	−45	0	+45	−20	0	+20	µA
Noninverting		+25°C	I	1	−25	+5	+35	−25	+5	+35	−13	+5	+18	µA
Input Bias Current TC[5]														
Noninverting		Full	IV		−50	+30	+125	−50	+30	+125	−50	+30	+125	nA/°C
Inverting		Full	IV		−50	+40	+130	−50	+40	+130	−50	+40	+130	nA/°C
Input Resistance														
Noninverting		+25°C	V			75			75			75		kΩ
Input Capacitance														
Noninverting		+25°C	V			1.5			1.5			1.5		pF
Common Mode Input Range	$T = T_{min}$	—	II	2	±1.0	±1.2		±1.0	±1.2		±1.0	±1.2		V
	$T = T_{min}$ to +25°C	—	II	1, 3	±1.4	±1.5		±1.4	±1.5		±1.4	±1.5		V
Common Mode Rejection Ratio		Full	II	4, 5, 6	50	60		50	60		50	60		dB
Power Supply Rejection Ratio	ΔV_S = ±5%	Full	II	4, 5, 6	50	60		50	60		50	60		dB
Open Loop Gain														
T_O	At dc	+25°C	V			3			3			3		MΩ
Nonlinearity	At dc	+25°C	V			5			5			5		ppm
Output Voltage Range		+25°C	II		±3.3	±3.7		±3.3	±3.7		±3.3	±3.7		V
Output Impedance	At dc	+25°C	V			0.08			0.08			0.08		Ω
Output Current (50 Ω Load)	$T = +25°C$ to T_{max}	—	II	1, 2	60			60			60			mA
	$T = T_{max}$	—	II	3	50			50			50			mA

AC ELECTRICAL CHARACTERISTICS (Unless otherwise noted, A_V = +10; $\pm V_S$ = ±5 V; R_f = 1 kΩ; R_{LOAD} = 100 Ω)

Parameter	Conditions	Temp	Test Level	Mil Sub[4]	AD9618JN/JR Min	AD9618JN/JR Typ	AD9618JN/JR Max	AD9618AQ/SQ/SZ/883B[4] Min	AD9618AQ/SQ/SZ/883B[4] Typ	AD9618AQ/SQ/SZ/883B[4] Max	AD9618BQ/TQ/TZ/883B[4] Min	AD9618BQ/TQ/TZ/883B[4] Typ	AD9618BQ/TQ/TZ/883B[4] Max	Units
FREQUENCY DOMAIN														
Bandwidth (−3 dB)														
Small Signal	$V_{OUT} \leq 2$ V p-p	Full	II	4, 5, 6	130	160		130	160		130	160		MHz
Large Signal	$V_{OUT} \leq 5$ V p-p	Full	IV			150		120	150		120	150		MHz
Bandwidth Variation vs. A_V	A_V = −1 to ±40	+25°C	V			35			35			35		MHz
Amplitude of Peaking (<50 MHz)	$T = T_{min}$ to +25°C	—	II	4, 5, 6		0			0	0.4		0	0.4	dB
	$T = T_{max}$	—	II	4, 5, 6		0			0	0.7		0	0.7	dB
Amplitude of Peaking (>50 MHz)	$T = T_{min}$ to +25°C	—	II	4, 5, 6		0			0	0.6		0	0.6	dB
	$T = T_{max}$	—	II	4, 5, 6		0			0	1.2		0	1.2	dB
Amplitude of Roll-Off (<75 MHz)		Full	II	4, 5, 6		0.5			0.5	1.2		0.5	1.2	dB
Phase Nonlinearity	dc to 75 MHz	+25°C	V			0.5			0.5			0.5		Degree
2nd Harmonic Distortion	2 V p-p; 4.3 MHz	Full	IV			−83	−75		−83	−75		−83	−75	dBc
	2 V p-p; 20 MHz	Full	IV			−63	−55		−63	−55		−63	−55	dBc
	2 V p-p; 60 MHz	Full	II	4, 5, 6		−51	−43		−51	−43		−51	−43	dBc
3rd Harmonic Distortion	2 V p-p; 4.3 MHz	Full	IV			−85	−77		−85	−77		−85	−77	dBc
	2 V p-p; 20 MHz	Full	IV			−70	−62		−70	−62		−70	−62	dBc
	2 V p-p; 60 MHz	Full	II	4, 5, 6		−62	−54		−62	−54		−62	−54	dBc
Input Noise Voltage	10 MHz	+25°C	V			1.2			1.2			1.2		nV/√(Hz)
Inverting Input Noise Current	10 MHz	+25°C	V			24			24			24		pA/√(Hz)

Parameter	Conditions	Temp	Test Level	Mil Sub*	AD9618JN/JR Min	Typ	Max	AD9618AQ/ SQ/SZ/883B* Min	Typ	Max	AD9618BQ/ TQ/TZ/883B* Min	Typ	Max	Units
Average Equivalent Integrated Input Noise Voltage	0.1 to 200 MHz	+25°C	V			38			38			38		μV, rms
TIME DOMAIN														
Slew Rate	V_{OUT} = 4 V Step	Full	IV			1800		1400	1800		1400	1800		V/μs
Rise/Fall Time														
V_{OUT} = 2 V Step		Full	IV			2.2			2.2	2.6		2.2	2.6	ns
V_{OUT} = 5 V Step	T = +25°C to	—	IV			2.3			2.3	2.8		2.3	2.8	ns
	T = T_{max}	—	IV			2.3			2.3	3.1		2.3	3.1	ns
Overshoot	V_{OUT} = 2 V Step	Full	IV			2			2	10		2	10	%
Settling Time														
To 0.1%	V_{OUT} = 2 V Step	Full	IV			9			9	15		9	15	ns
To 0.02%	V_{OUT} = 2 V Step	Full	IV			14			14	23		14	23	ns
To 0.1%	V_{OUT} = 4 V Step	Full	IV			10			10	16		10	16	ns
To 0.02%	V_{OUT} = 4 V Step	Full	IV			16			16	24		16	24	ns
2×Overdrive Recovery to ±2 mV of Final Value	V_{IN} = 0.6 V Step	+25°C	V			50			50			50		ns
Propagation Delay		+25°C	V			2			2			2		ns
Differential Gain[7]		Full	V			0.01			0.01			0.01		%
Differential Phase[7]		Full	V			0.02			0.02			0.02		Degree
POWER SUPPLY REQUIREMENTS														
Quiescent Current														
$+I_s$		Full	II	1, 2, 3		31	43		31	43		31	43	mA
$-I_s$		Full	II	1, 2, 3		31	43		31	43		31	43	mA

For applications help, call Computer Labs Division at (919) 668-9511.

NOTES

[1]Absolute maximum ratings are limiting values to be applied individually and beyond which the serviceability of the circuit may be impaired. Functional operability is not necessarily implied. Exposure to absolute maximum rating conditions for an extended period of time may affect device reliability.

[2]Output is short circuit protected to ground, but not to supplies. Continuous short circuit to ground may affect device reliability.

[3]Typical thermal impedances (part soldered onto board):
Mini-DIP: θ_{JA} = 140°C/W; θ_{JC} = 30°C/W.
Side Brazed/Cerdip: θ_{JA} = 110°C/W; θ_{JC} = 20°C/W.
SOIC Package: θ_{JA} = 150°C/W; θ_{JC} = 30°C/W.
Ceramic Gull Wing: θ_{JA} = 120°C/W; θ_{JC} = 20°C/W.

[4]Military subgroups apply only to military qualified devices.

[5]Measured with respect to the inverting input.

[6]Typical is defined as the mean of the distribution.

[7]Frequency = 4.3 MHz; R_L = 150 Ω; A_V = +10.

*Contact factory regarding MIL-883 parts in "Z" packages.

Specifications subject to change without notice.

EXPLANATION OF MILITARY SUBGROUPS

Subgroup 1 – Static tests at +25°C.
(5% PDA calculated against Subgroup 1 for high-rel versions.)
Subgroup 2 – Static tests at maximum rated operating temperature.
Subgroup 3 – Static tests at minimum rated operating temperature.
Subgroup 4 – Dynamic tests at +25°C.
Subgroup 5 – Dynamic tests at maximum rated operating temperature.
Subgroup 6 – Dynamic tests at minimum rated operating temperature.
Subgroup 7 – Functional tests at +25°C.
Subgroup 8 – Functional tests at maximum and minimum rated temperatures.
Subgroup 9 – Switching tests at +25°C.
Subgroup 10 – Switching tests at maximum rated operating temperature.
Subgroup 11 – Switching tests at minimum rated operating temperature.
Subgroup 12 – Periodically sample tested.

EXPLANATION OF TEST LEVELS

Test Level

I – 100% production tested.
II – 100% production tested at +25°C and sample tested at specified temperatures. AC testing of J grade devices done on sample basis.
III – Sample tested only.
IV – Parameter is guaranteed by design and characterization testing.
V – Parameter is a typical value only.
VI – All devices are 100% production tested at +25°C. 100% production tested at temperature extremes for extended temperature devices; sample tested at temperature extremes for commercial/industrial devices.

ORDERING INFORMATION

Model	Temperature Range	Package
AD9618JN	0 to +70°C	Plastic DIP
AD9618JR	0 to +70°C	SOIC
AD9618AQ	−40°C to +85°C	Cerdip
AD9618BQ	−40°C to +85°C	Cerdip
AD9618SQ	−55°C to +125°C	Cerdip
AD9618TQ	−55°C to +125°C	Cerdip
AD9618SQ/883B	−55°C to +125°C	Cerdip
AD9618TQ/883B	−55°C to +125°C	Cerdip
AD9618SZ*	−55°C to +125°C	Ceramic Gull Wing
AD9618TZ*	−55°C to +125°C	Ceramic Gull Wing

*Contact factory regarding MIL-883 parts in "Z" packages.

E.3 Computer Program Listings

- Hspice frequency analysis of the magnetic probe

```
FEQUENCY ANALYSIS OF THE MAGNETIC FIELD SENSOR
**************************************
* THIS IS THE SOURCE SETUP
**************************************
vin     1 0 ac  1
cin     1 2 1e-15
rin     2 0 1
ein1     3 0 2 0   6e6
ein2     7  0 2 0 -6e6
*-------------------------------------
*probe antenna + transformer
*-------------------------------------
la1       3    4     1.26m          $measured loop antenna inductance
ra1       4    5     128m           $measured loop antenna resistance
rp1       5    0     217.6k         $due to the losses in the rod
ca1       5    0     55.4f          $interwinding antenna capacitance
rw1       5    9     23.9m          $second. winding resistance
lse1      5    6     1.48e-4        $parallel induc. of the toroid(mat.75)
cw1       5    0     10.6p          $second. winding capacitance
rse1      6    0     915            $losses due to eddy current&hysterisis
la2       7    8     1.26m          $measured loop antenna inductance
ra2       8    21    128m           $measured loop antenna resistance
rp2       21   0     217.6k         $due to losses in the rod
ca2       21   0     55.4f          $second. winding resistance
rw2       21   11    20.7m          $second. winding resistance
lse2      21   22    1.877e-4       $parallel induc. of the toroid(mat.75)
cw2       21   0     7.8p           $second. winding capacitance
rse2      22   0     1184           $losses due to eddy current&hysterisis
*-------------------------------------
*operational amplifiers(balanced conf.)
*-------------------------------------
x1op 9  17  12 100 90 op37
x2op 11 19  13 100 90 op37
x3ad 15 14 out 100 90 ad9618
.model   op37     amp
+ srpos=17x srneg=17x ib=20.00n ibos=15n
+vos=30.00u freq=63x delphs=71 cmrr=122 rout=70
+av=1x isc=50m vopos=3.7 voneg=-3.7 pwr=100m
+vcc=5.00 vee=-5.0 temp=25.00 psrr=114
****************************************
.model   ad9618   amp
+ srpos=1800x srneg=1800x ib=0.5u
+vos=0.5m freq=160x delphs=50 cmrr=60 rout=0.08
+av=3x isc=70m vopos=3.7 voneg=-3.7 pwr=300m
+vcc=5.00 vee=-5.0 temp=25.00 psrr=60
****************************************
c112   9    12  5.6p
r112   9    12  272
r170   17    0  272
c213   11   13  5.6p
r213   11   13  272
r190   19    0  272
r74    13   14  162
r85    12   15  162
r40    14    0  1000
```

```
r56     15   40   1000
r154    40   out  39.2
rload   out   0   50
.options  nomod   post=1
.ac dec 20 1e1 5e7
.meas maxvalue max vdb(out) from=1e1 to=1e5
.meas freq-3db1 when vdb(out)=-38.62
.meas freq-3db2 when vdb(out)=-38.62 td=1xhz
.meas freq45 when vp(out,0)=-45 td=1xhz
.print  vdb(out) vp(out,0)
.end
```

- Hspice transient analysis of the magnetic probe

```
TRANSIENT ANALYSIS OF THE MAGNETIC FIELD SENSOR
*****************************************
* THIS IS THE SOURCE SETUP
*****************************************
vin     in   0   pu(0 1 0 70n 70n 620n  1u)
*vin    in   0   sin(0 1 60 0 0 0)
cin     in   2   1e-15
rin     2 0 1
ein1     3 0 2 0    6e6
ein2     7  0 2 0 -6e6
*-----------------------------------------
*probe antenna + transformer
*-----------------------------------------
la1      3    4     1.26m       $measured loop antenna inductance
ra1      4    5     128m        $measured loop antenna resistance
rp1      5    0     217.6k      $due to the losses in the rod
ca1      5    0     55.4f       $interwinding antenna capacitance
rw1      5    9     23.9m       $second. winding resistance
lse1     5    6     1.48e-4     $parallel induc. of the toroid(mat.75)
cw1      5    0     10.6p       $second. winding capacitance
rse1     6    0     915         $losses due to eddy current&hysterisis
la2      7    8     1.26m       $measured loop antenna inductance
ra2      8    21    128m        $measured loop antenna resistance
rp2      21   0     217.6k      $due to losses in the rod
ca2      21   0     55.4f       $interwinding antenna capacitance
rw2      21   11    20.7m       $second. winding resistance
lse2     21   22    1.877e-4    $parallel induc. of the toroid(mat.75)
cw2      21    0    7.8p        $second. winding capacitance
rse2     22    0    1184        $losses due to eddy current&hysterisis
*-----------------------------------------
*operational amplifiers(balanced conf.)
*-----------------------------------------
x1op 9  17  12  100 90 op37
x2op 11 19  13  100 90 op37
x3ad 15 14  out 100 90 ad9618
.model    op37      amp
+ srpos=17x srneg=17x ib=20.00n ibos=15n
+vos=30.00u freq=63x delphs=71 cmrr=122 rout=70
+av=1x isc=50m vopos=3.7 voneg=-3.7 pwr=100m
+vcc=5.00 vee=-5.0 temp=25.00 psrr=114
*****************************************
.model    ad9618    amp
+ srpos=1800x srneg=1800x ib=0.5u
+vos=0.5m freq=160x delphs=50 cmrr=60 rout=0.08
+av=3x isc=70m vopos=3.7 voneg=-3.7 pwr=300m
+vcc=5.00 vee=-5.0 temp=25.00 psrr=60
*****************************************
c112    9    12   5.6p
r112    9    12   272
r170    17    0   272
c213    11   13   5.6p
r213    11   13   272
r190    19    0   272
r74     13    14  162
r85     12   15   162
```

```
r40     14    0   1000
r56     15   40   1000
r154    40   out   39.2
rload   out   0   50
.options  nomod   post=1
.tran 4ns 1u
.param va=24.27m  vb=11m
.meas tran risetime trig v(out) val='vb'  rise=1
+          targ v(out) val='0.9*va'   rise=1
.meas falltime trig v(out) val='0.9*va'  fall=1
+   td=400ns    targ v(out) val='vb'  fall=1
.print  v(out)
.end
```

Bibliography

[1] A. D. Watt , "VLF radio engineering," Vol. 14 Pergamon Press, pp. 413-431. 1967.

[2] Analog Devices, "Linear products data book 1988," Analog Devices Inc., 1988.

[3] C. E. Baum, Edward L. Breen, Felix L. Pitts, Gary D. Sower, Mitchel E. Thomas, "The measurement of lightning environmental parameters related to interaction with electronic systems," IEEE Trans. EMC, Vol. EMC-24, No. 2, pp. 123-137, May 1982.

[4] C. E. Baum, Edward L. Breen, Joseph C. Giles, John O' Neil, Gary D. Sower, "Sensors for electromagnetic pulse measurements both inside and away from nuclear source regions," IEEE Trans. EMC, Vol. EMC, No. 1, pp. 22-35, February 1978.

[5] C. E. Baum, "The multiple Moebius strip loop," Sensor and Simulation Notes, Note XXV. US Air Force Laboratory, August 1966.

[6] C. E. Baum, "The multi-gap cylindrical loop in non-conducting media," Sensor and Simulation Notes, Note XLI, US Air Force Laboratory, May 1967.

[7] C. E. Baum, "A conical-transmission-line gap for a cylindrical loop," Sensor and Simulation Notes, Note XLII, May 1967.

[8] C. E. Baum, "Some considerations for electrically-small multi-turn cylindrical loops", Sensor and Simulation Notes, Note XLIII, US Air Force Laboratory,

May 1967.

[9] C. E. Baum, "Further considerations for electrically-small multi-turn cylindrical loops," Sensor and Simulation Notes, Note XLIII, US Air Force Laboratory, April 1971.

[10] D. E. Barrick, "Miniloop antenna operation and equivalent circuit," IEEE Trans. on Antennas and Propagation, Vol. AP-34, No. 1, pp. 111-114, January 1986.

[11] D. G. Lukoschus, "Optimization theory for induction-coil magnetometers at higher frequencies," IEEE Trans. on Geoscience Electronics, Vol. GE-17, No. 3, pp. 56-63, July 1979.

[12] D. Hoff, "An universal applicable field strength measuring probe for LF, MF, and HF bands," International Symposium on EMC, pp. 125-128, October 1984.

[13] E. C. Snelling, A. D. Giles, "Ferrites for inductors and transformers," Research Studies Press Ltd., 1983.

[14] E. J. Kennedy, "Operational amplifier circuits, theory and applications," Holt, Rinehart and Winston, Inc., 1988.

[15] Fair-Rite Products Corp., "Fair-Rite linear ferrites cathalog," 10^{th} Edition.

[16] F. M. Tesche, "Numerical determination of the spacing of N loops for minimum inductance in $\dot{B}$ sensor," IEEE Trans. on Inst. and Meast., Vol. IM-24, No. 3, pp. 243-246, September 1975.

[17] G. S. Smith, "Loop antennas," Antenna Engineering Handbook, Second Edition, Richard C. Johnson, Henry Jasik, eds., McGraw-Hill Inc., 1984, pp. 5.1-5.24.

[18] H. A. Whefler, "Small antennas," IEEE Trans. on Antennas and propagation, Vol. AP-23, No. 4, pp. 462-469, July 1975.

[19] Hewlett Packard, "3577A network analyzer, 35677 A/B S-parameter test set operating manual," Hewlett-Packard Company, 1983.

[20] H. Whiteside, R. W. P. King, "The loop antenna as a probe," IEEE Trans. on Antennas and Propagation, pp. 291-297, May 1964.

[21] H. W. Ott, "Noise reduction techniques in electronic systems," Second Edition, A Wiley-Interscience Publication, pp. 60-70, 1988.

[22] M. S. Di Capua, "High speed magnetic field and current and Current measurements," Fast Electrical and Optical Measurements, volume 1, J. E. Thompson and L. H. Luessen, eds., Martinus Nijhoff publishers, Dordrecht, pp. 223-262, 1986.

[23] J. P. Castillo and L. Marin, "Measurements of system responses to transient exitations," Time-Domain Measurements in Electromagnetics, Edmund K. Miller, eds., Van Nostrand Reinhold, co, pp. 268-295, 1986.

[24] J. P. Hauser, "A 20-Hz-to-200KHz magnetic field probe for EMI surveys," IEEE Trans. EMC, Vol. EMC-32, No. 1, pp. 67-69, February 1990.

[25] K. P. Esselle, S. S. Stuchly, "Resistively loaded loop as a pulse-receiving antenna," IEEE Trans. on Antennas and Propagation, Vol. 38, No. 7, pp. 1123-1126, July 1990.

[26] L. D. Driver, M. Kanda, "An optically linked electric and magnetic field sensor for poynting vector measurements in the near fields of radiating sources," IEEE Trans. EMC, Vol. EMC-30, No. 4, pp. 495-503, November 1988.

[27] M. A. Stuchly, D. T. Gibbons, A. Thansandote, H. LePocher, "Magnetic field sensor for measurement of transients," Proc. CPEM, Ottawa. June 1990.

[28] M. A. Stuchly, S. S. Stuchly, "Measurements of electromagnetic fields in biomedical applications," CRC Critical Reviews in Biomedical Engineering, Vol. 14, Issue 3, pp. 241-288.

[29] Meta Software, "Hspice users' manual H8801," Meta-Software, Inc., 1985.

[30] M. L. Crawford, "Generation of standard EM fields using TEM transmission cells," IEEE Trans. EMC, Vol. EMC-16, No. 4, pp. 189-195, November 1974.

[31] M. L. Crawford, J. Workman, C. L. Thomas, "Expanding the bandwith of TEM cells for EMC measurements," IEEE Trans. EMC, Vol. EMC-20, No. 3, pp. 368-375, August 1978.

[32] M. E. Van Valkenburg, "Analog filter design," Holt, Rinehart and Winston Company, 1982, pp. 119-143.

[33] M. J. Johnson, E. L. Bronaugh, "Small electromagnetic field sensors- An overview," IEEE Int. Symp. EMC, pp. 140-145, September 1982.

[34] N. R. Grossner, I. S. Grossner, "Transformers for electronic circuits," Second Edition, McGraw-Hill Inc., 1983.

[35] P. H. Ducan, JR., "Analysis of a Moebuis loop magnetic field sensor," IEEE Trans. EMC, Vol. EMC-16, No. 2, pp. , May 1974.

[36] P. Horowitz, W. Hill, "The art of electronics," Second Edition, Cambridge University Press, 1989, pp391-445.

[37] P. W. Tuinenga, "Spice: A guide to circuit simulation and analysis using Pspice," Prentice Hall Inc., 1988.

[38] P. F. Wilson, D. C. Chang, M. T. Ma, "Input impedance of a probe antenna in a TEM cell," IEEE Trans. EMC, Vol. EMC-26, No. 3, pp. 154-161, November 1984.

[39] R. Arseneau, J. J Zelle, "A tri-axis electromagnetic field meter," IEEE trans. on Inst. meast., Vol 39, No. 1, pp. 23-26, February 1990.

[40] R. Lee, L. Wilson, C. E. Carter, "Electronic transformers and circuits," Third Edition, John Wiley and Sons, Inc., 1988.

[41] R. Mauro, "Engineering electronics, a practical approach," Prentice Hall Inc., 1989, pp. 455-509.

[42] R. J. Spiegel, C. A. Booth, E. L. Bronaugh, "A radiation measuring system with potential automotive under-hood application," IEEE Trans. EMC, Vol. EMC-25, No. 2, pp. 61-69, May 1983.

[43] R. J. Spiegel, W. T. Joines, C. F. Blackman, A. W. Wood, "A method for calculating electric and magnetic fields in TEM cells at ELF," IEEE Trans. EMC, Vol. EMC-29, No. 4, pp. 265-272, November 1987.

[44] R. C. Pettengili, H. T. Garland, J. D. Meindl, "Receiving antenna design for miniature receivers," IEEE Trans. on Antennas and Propagation, Vol. AP-25, No. 4, pp. 528-534, July 1977.

[45] R. DeVore, P. Bohley, "The electrically small magnetically loaded multiturn loop antenna," IEEE Trans. on Antennas and Propagation, Vol. AP-25, No. 4, pp. 496-505, July 1977.

[46] S. A. Macintyre, "A portable low noise low frequency three axis search coil magnometer," IEEE Trans. Mag., Vol.MAG-16, No. 5, pp. 761-763, September 1980.

[47] S. Iskra, I. P. Macfarlane, "H-field sensor measurement errors in the near field of a magnetic dipole source," IEEE Trans. EMC, Vol. EMC-31, No 3, pp. 306-311, August 1989.

[48] Tektronix, "The 11800 series digital sampling oscilloscopes," Tektronix, Inc., 1989.

[49] T. S. M. Maclean, "Principles of antennas wire and aperature," Prentice Hall Inc., 1986, pp. 84-103. January 1986.

[50] United Nations Environment Program, the World Health Organization and the International Radiation Protection Association (IRPA), "Magnetic fields", World Health Organizations, Geneva 1987.

[51] V. G. Welsby, "The theory and design of inductance coils," McDonald and Co. Ltd., 1960

[52] W. D. Stanley, "Operational amplifiers with linear integrated circuits," Second Edition, Merill Publishing Company, 1989.

[53] Y. G. Chen, R. Crumley, S. LLoyd, C. E. Baum, D. V. Giri, "Field-containing inductors," IEEE Trans. EMC, Vol. EMC-30, No. 3, pp. , August 1988.